

Visual interpretation of the robustness of Non-Negative Associative Gradient Projection Points over function minimizers in mini-batch sampled loss functions

Dominic Kafka¹ and Daniel Wilke¹

¹Centre for Asset and Integrity Management (C-AIM), Department of Mechanical and Aeronautical Engineering, University of Pretoria, Pretoria, South Africa
{*dominic.kafka@gmail.com,wilkedn@gmail.com*}

March 21, 2022

Abstract

Mini-batch sub-sampling is likely here to stay, due to growing data demands, memory-limited computational resources such as graphical processing units (GPUs), and the dynamics of on-line learning. Sampling a new mini-batch at every loss evaluation brings a number of benefits, but also one significant drawback: The loss function becomes discontinuous. These discontinuities are generally not problematic when using fixed learning rates or learning rate schedules typical of subgradient methods. However, they hinder attempts to directly minimize the loss function by solving for critical points, since function minimizers find spurious minima induced by discontinuities, while critical points may not even exist. Therefore, finding function minimizers and critical points in stochastic optimization is ineffective. As a result, attention has been given to reducing the effect of these discontinuities by means such as gradient averaging or adaptive and dynamic sampling. This paper offers an alternative paradigm: Recasting the optimization problem to rather find Non-Negative Associated Gradient Projection Points (NN-GPPs). In this paper, we demonstrate the NN-GPP interpretation of gradient information is more robust than critical points or minimizers, being less susceptible to sub-sampling induced variance and eliminating spurious function minimizers. We conduct a visual investigation, where we compare function value and gradient information for a variety of popular activation functions as applied to a simple neural network training problem. Based on the improved description offered by NN-GPPs over minimizers to identify true optima, in particular when using smooth activation functions with high curvature characteristics, we postulate that locating NN-GPPs can contribute significantly to automating neural network training.

Keywords: Artificial Neural Networks, Gradient-only, Minima, Activation Functions

1 Introduction

Growing data demands, memory limited efficient computational resources, such as graphical processing units (GPUs), and the dynamic world of on-line learning, make avoiding mini-batch sub-sampling unlikely. In mini-batch sub-sampled computed loss functions for neural networks, the resulting loss function is discontinuous when the mini-batch changes for every evaluation of the loss function. Benefits of changing the mini-batch sub-sampling at every evaluation include overcoming weaker local basins of attraction [Kleinberg et al., 2018], in addition to acting as an effective regularizer to obtain better generalizable solutions [Masters and Luschi, 2018]. However, a significant drawback is

introduced, namely a resulting discontinuous loss function. Although discontinuous loss functions are in general not a problem when selecting fixed learning rates or fixed learning rate schedules, typical of subgradient methods [Shor, 1985]. They do, however, hinder attempts to directly minimize the function by line search minimization for example, or at finding candidate minimizers by solving for critical points¹. This is due to function minimizers being susceptible to finding spurious minima induced by these discontinuities, while critical points typically do not exist. This renders both predominant mathematical programming paradigms for finding finding (candidate) minimizers by direction minimization or critical points, ineffective when considering stochastic optimization. As a result, significant effort has been invested in reducing or eliminating the effect of these discontinuities by means of adaptive and dynamic (recursive) sampling [Kashyap et al., 1970, Csiba and Richtarik, 2018]. This paper suggests an alternative paradigm to enhance the quality of information before considering to increase batch sizes, namely, to recast the optimization problem to rather find non-negative associated gradient projection points (NN-GPPs). NN-GPPs are solutions to the recently formalized gradient-only optimization problem [Wilke et al., 2013b, Snyman and Wilke, 2018], which have been demonstrated to be a robust solution to discontinuous functions resulting from remeshing in finite element based structural shape optimization [Wilke et al., 2013b]. In the structural shape problem, as the geometrical shape of a structure changes, the discretization or mesh used to resolve the objective and constraint functions changes. Since the objective and constraint functions are resolved by solving mixed Algebraic and partial differential equation based governing equations (that define structural equilibrium) non-smooth or abrupt changes in remeshing introduce discontinuities. Inferior solutions are often computed, as a direct result of these discontinuities, using mathematical programming solvers. Consequently, the majority of research in structural shape optimization aimed at reducing the size of these discontinuities by resolving solutions on very fine meshes. However, this led to excessively expensive computational solutions, which the recently proposed gradient-only optimization problem solved Wilke et al. [2013a]. NN-GPPs have been formalized on a rigorous mathematical foundation and proven to be equivalent to semi-positive definite local minimizers for twice continuously differentiable smooth functions [Wilke et al., 2013b]. A whole range of gradient-only line search optimizers to locate NN-GPP have been proposed [Wilke et al., 2013b, Snyman and Wilke, 2018]. This study recognizes that gradient-only optimization to overcome the difficulties associated with discontinuities in shape optimization may be as effective to overcome the difficulties associated with discontinuities induced by mini-batch sampling as motivated by the following illustrative example.

Consider finding the optimum of a quadratic function, where the underlying quadratic function is estimated from a data set, as depicted in Figure 1. Utilizing all the data, i.e. using the full batch, to resolve the quadratic function gives the true quadratic function, depicted as a blue dashed line. Alternatively, the full batch can be split into numerous mini-batches. In this example we consider four mini-batches. Estimating the quadratic model using any of the individual mini-batches resolves different quadratic functions, where each quadratic function has its own apparent minimum as well as associated value. Suppose now that a new quadratic function is constructed by an oracle [Agarwal et al., 2012], that randomly selects one of the four batches every time the quadratic function or derivative is evaluated for a specific x as shown in Figure 1(c) and (d). The consequence is that the oracle constructed quadratic function is discontinuous, though the sampled black dots are connected in the diagram to visually aid the discussion. Consider the local minima depicted as red dots in Figure 1(c) versus NN-GPP depicted as red dots in Figure 1(d). A NN-GPP is simply identified as a sign change in the directional derivative from negative to positive as we move along a descent direction. This will become apparent from the formalization offered later in this study.

¹i.e. points at which the gradient are zero

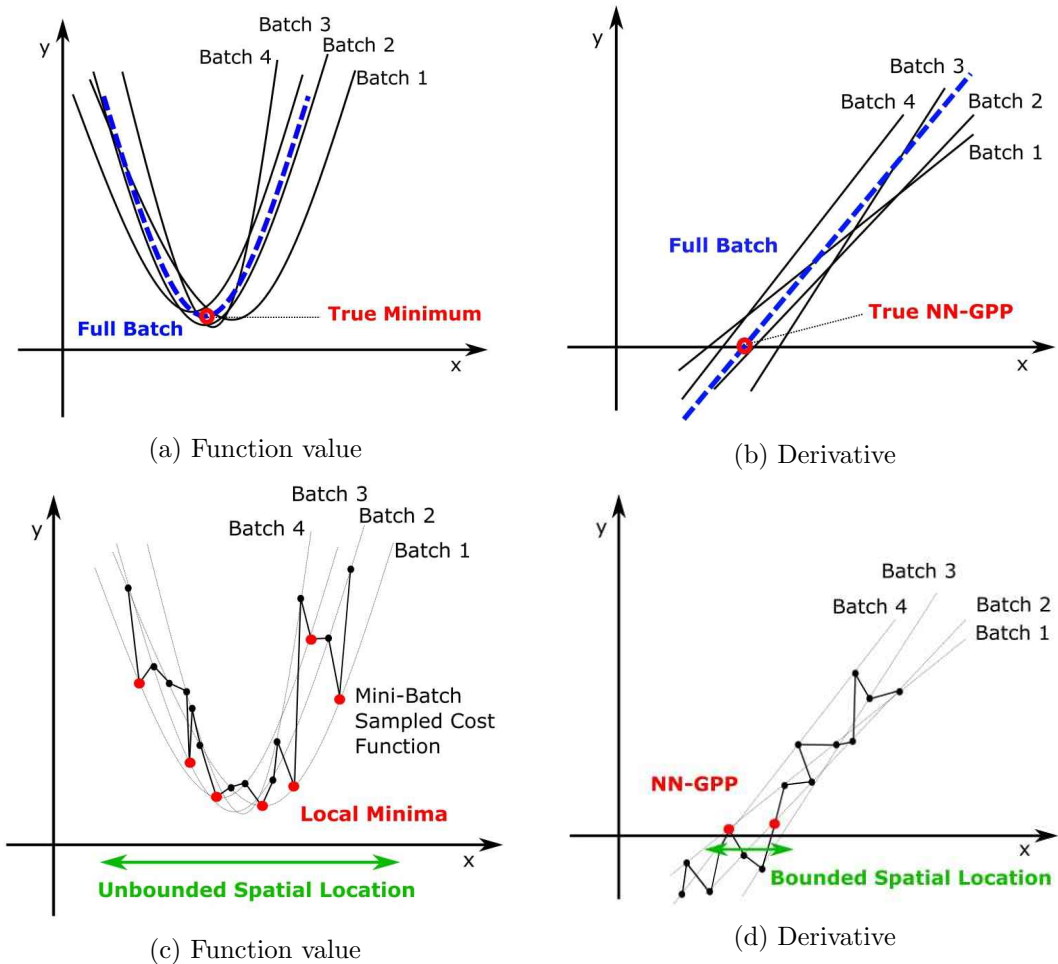


Figure 1: Conceptual depiction of the mini-batch problem and the utility of the NN-GPP definition. The full batch expression is the average of 4 different batches, which themselves construct own expressions of the loss function and derivative, each with different characteristics. When sampling randomly between these fixed batches, the function value and derivative "jumps" between the quadratics corresponding to the different batches. Connecting these jumps creates the non-smooth function value and derivative functions. Minimum definitions result in candidate points that are unbounded in spatial location along x . Conversely, NN-GPP candidate points remain bounded, as long as the curvature of the function is non-trivial and the variance due to sub-sampling is bounded.

Four observations are noteworthy, i) apparent solutions of the NN-GPP are much more localized around the true or full batch solution, ii) every NN-GPP solution is also a minimizer (i.e. present as a red dot in Figure 1(c)), iii) majority of the minimizers in Figure 1(c) are completely ignored in Figure 1(d), iv) the spatial variance of the NN-GPPs are representative of the uncertainty relating to the full batch solution, whereas the spatial variance of the minimizers is poorly related to the full batch solution. In a recent study a basic line search to find NN-GPP [Kafka and Wilke, 2019] proved promising and yielded competitive results when compared to Bayesian stochastic line searches [Mahsereci and Hennig, 2017].

This study aims to explore and investigate the implication of activation functions on the nature of the loss and gradient functions, which ultimately translates to an understanding of the potential for finding NN-GPP as opposed to minimizers in neural network training. Although many studies have been done on neural network loss functions in either a theoretical [Nguyen et al., 2018, Liang et al., 2018] or visual context [Goodfellow et al., 2015, Li et al., 2018, Im et al., 2016], most studies concentrate on the

convexity properties with regards to function value of the loss function in expectation or the full batch setting. Given how much emphasis optimization strategies put on gradient information, it is sensible to pay closer attention to the landscape in which most training strategies operate [Robbins and Monro, 1951, Kingma and Ba, 2015, Duchi et al., 2011], as well as how they are influenced by activation functions (AFs). To the best of our knowledge this is the first study to visually explore the qualitative characteristics of gradient or directional derivative information in stochastically sub-sampled loss functions of neural networks. Thus we investigate the qualitative performance of minima and NN-GPP definitions as applied to stochastic loss functions associated with different activation functions. We choose a visual approach to do so, such that an intuitive understanding of the relationship between mini-batch sampling, minima and NN-GPPs as well as activation functions [Serwa, 2017, Karlik, 2015, Laudani et al., 2015] can be developed. As we take you our reader on this visual tour, we would like to remind you to keep the following question: **What is the quality of the information to make informed decisions on candidate solutions in mini-batched sampled neural network training?** - in the back of your mind, as we work through the paper on characteristics of function values and directional derivatives for different activation functions.

1.1 Our contribution

The novelty of this work lies neither in the dataset, nor the network architecture. We wish to draw attention to the information used to analyze potential optima, and wish to build an intuitive and visual understanding of function minimizers versus NN-GPP when dealing with mini-batched sampled loss functions. Hence, we restrict this study to an elementary neural network classification problem in order to highlight concepts with absolute clarity. We show that function minimization in stochastic loss functions is not effective. Instead, gradient-only optimization that finds *Non-Negative Associative Gradient Projection Points* (NN-GPPs) allows for a much improved representation of the full batch optima. We demonstrate this for neural networks loss functions using the Sigmoid, Tanh, Softsign, ReLU, leaky ReLU and ELU activation functions. We also highlight some key differences between the features of the loss functions with the different activations in the context of NN-GPP. We show that the shape of the activation function and consequently its derivative affects the localization of NN-GPP in weight space.

2 The stochastic optimization problem

The loss function used in neural network training commonly takes the form of

$$\mathcal{L}(\mathbf{x}) = \frac{1}{M} \sum_{k=1}^M \ell(\mathbf{x}; \mathbf{t}_k), \quad (1)$$

where $\{\mathbf{t}_1, \dots, \mathbf{t}_k\}$ is training dataset of M samples, and the model parameters are given by vector $\mathbf{x} \in \mathcal{R}^d$. The loss quantifying the adequacy of parameters \mathbf{x} in terms of training data \mathbf{t} is given by $\ell(\mathbf{x}; \mathbf{t})$. The true or full batch gradient with regards to parameters \mathbf{x} is given by

$$\nabla \mathcal{L}(\mathbf{x}) = \frac{1}{M} \sum_{k=1}^M \nabla \ell(\mathbf{x}; \mathbf{t}_k), \quad (2)$$

and can be computationally efficiently calculated using backpropagation [Werbos, 1994]. In the case where all the training data is used for function and gradient evaluations, $\mathcal{L}(\mathbf{x})$ is continuous, while the continuity of $\nabla \mathcal{L}(\mathbf{x})$ depends on the continuity and smoothness of the AF used.

A local minimum of a loss function for full batch sampling is defined as follows:

Definition 2.1. Local Minimum: Let \mathbf{x}^* be a local minimum of $\mathcal{L}(\mathbf{x})$, such that

$$\nabla \mathcal{L}(\mathbf{x}) = \mathcal{L}(\mathbf{x}) - \mathcal{L}(\mathbf{x}^*) \geq 0, \quad (3)$$

for any point \mathbf{x} in the neighborhood of \mathbf{x}^* [Arora, 2011].

However, machine learning training is rarely conducted using full batches. Instead, the use of a smaller number of samples or mini-batches have become common practice, i.e. $\mathcal{B} \in \{1, \dots, M\}$, with $|\mathcal{B}| \ll M$. Note, here we consider a re-evaluation of the mini-batch for every function evaluation. This changes the loss function and its gradient computation to the following approximate form:

$$L(\mathbf{x}) = \frac{1}{|\mathcal{B}|} \sum_{k \in \mathcal{B}} \ell(\mathbf{x}; \mathbf{t}_k), \quad (4)$$

and

$$\mathbf{g}(\mathbf{x}) = \frac{1}{|\mathcal{B}|} \sum_{k \in \mathcal{B}} \nabla \ell(\mathbf{x}; \mathbf{t}_k). \quad (5)$$

These approximations have expectation $\mathbb{E}[L(\mathbf{x})] = \mathcal{L}(\mathbf{x})$ and $\mathbb{E}[\mathbf{g}(\mathbf{x})] = \nabla \mathcal{L}(\mathbf{x})$ [Tong and Liu, 2005]. However, significant variations from the mean can be observed between individual batches \mathcal{B} . This has the consequence, that the first order optimality criterion $\mathbf{g}(\mathbf{x}^*) = \mathbf{0}$ [Arora, 2011], i.e. the existence of a critical point at \mathbf{x}^* may not exist for mini-batches although it does exist for the full batch, i.e. $\nabla \mathcal{L}(\mathbf{x}^*) = \mathbf{0}$.

We therefore distinguish between an apparent local minimum, and a true local minimum as follows:

Definition 2.2. True Local Minimum: A true local minimum is a minimum, \mathbf{x}^* , present when the full-batch loss function is evaluated $\mathcal{L}^* = \mathcal{L}(\mathbf{x}^*)$, while an apparent minimum, \mathbf{x}^{*a} , is a minimum that is present when the mini-batch evaluated loss function $L^{*a} = L(\mathbf{x}^{*a})$ is evaluated.

Lastly, a *Non-Negative Associative Gradient Projection Point* (NN-GPP) [Wilke et al., 2013b, Snyman and Wilke, 2018] to define optimality for discontinuous functions is given by:

Definition 2.3. NN-GPP: A NN-GPP is defined as any point, \mathbf{x}_{nngpp} , for which there exists $\epsilon_{max} > 0$ such that

$$\mathbf{d} \cdot \mathbf{g}(\mathbf{x}_{nngpp} + \epsilon \mathbf{d}) \geq 0, \quad \forall \mathbf{d} \in \{\mathbf{y} \in \mathcal{R}^n \mid \|\mathbf{y}\|_2 = 1\}, \quad \forall \epsilon \in (0, \epsilon_{max}]. \quad (6)$$

We offer the following three observations. Firstly, this implies that the directional derivative along any direction pointing away from \mathbf{x}_{nngpp} is non-negative, which implies that the function is not decreasing according to the gradient information. Hence, a NN-GPP incorporates second order information, i.e. identifies a minimum based purely on evidence from gradient information. Secondly, for twice continuously differentiable smooth functions every NN-GPP is also a semi-positive definite critical point [Wilke et al., 2013b] or local minimizer. Thirdly, when approaching a NN-GPP that is unique within its neighbourhood along any arbitrary direction, the directional derivative along the direction will change sign from negative (descent) to positive (ascent) at the NN-GPP.

3 Function and directional derivative surface visualization

Subsequently, we explore the quality of function value and gradient information together with the various optimality formulations within the context of an elementary neural network problem.

For this investigation we construct the loss functions for training a small neural network on the classic Iris dataset. We use a fixed architecture of a fully connected feed forward neural network with a single hidden layer containing 10 hidden units. The loss function used is the Mean Squared Error (MSE). The presented figures were generated using a 100x100 grid of both function value and gradient vector evaluations. In this section the axes denote steps along two random but perpendicular unit directions [Li et al., 2018], \mathbf{d}_1 and \mathbf{d}_2 , in \mathcal{R}^n , where n is the number of weights in the network, which is $n = 83$. The directional derivatives were calculated using the positive diagonal, i.e. the sum of the two unit directions, given as follows:

$$\mathbf{d}_{dd} = \frac{(\mathbf{d}_1 + \mathbf{d}_2)}{\|\mathbf{d}_1 + \mathbf{d}_2\|_2}. \quad (7)$$

Every directional derivative in the 100x100 grid is evaluated by projecting each computed gradient vector onto the normalized diagonal direction \mathbf{d}_{dd} , i.e. $\mathbf{g}(\mathbf{x})^T \cdot \mathbf{d}_{dd}$, which allows this scalar field of directional derivatives to be visualized as a surface.

The computed loss functions of the various activation functions are evaluated in a grid with range of $[-20, 20]$ units in the directions \mathbf{d}_1 and \mathbf{d}_2 around this point. Independent of the activation function, the centroid \mathbf{x}_0 and directions, \mathbf{d}_1 and \mathbf{d}_2 , remain constant, which allows us to isolate the variations due to only the activation functions. Care should also be exercised in interpreting these two dimensional visualizations of an 83-dimensional problem, as what seems to be a local minima on these two dimensional surfaces may well have descent directions leading from these low dimensional optima in some other directions not depicted.

The first visualization, using the Sigmoid activation function (AF) can be seen in Figure 2. We plot the function value and directional derivatives for batch sizes $\mathcal{B} \in \{150, 149, 10, 1\}$, where $\mathcal{B} = 150$ signifies the full batch. The full batch surface of both the function value and the directional derivative are perfectly smooth. By only omitting one random sub-sample, the function value surface becomes discontinuous. These discontinuities are caused by omitting a different sub-sample for every function evaluation². In comparison, the apparent variance in the discontinuous directional derivative surface is much lower than the discontinuous function surface. As the batch size is reduced to $\mathcal{B} = 10$, the true structure of the function surface is largely lost in the high variance caused by discontinuities. This trend becomes exaggerated, as the batch is reduced further to $\mathcal{B} = 1$.

We offer an explanation to this observation in the following discussion: Consider our case, where the loss function is the mean squared error:

$$\ell(\mathbf{x}; \mathbf{t}_k^i) = \frac{1}{2}(\mathbf{t}_k^o - \hat{\mathbf{y}}(\mathbf{t}_k^i, \mathbf{x}))^2, \quad (8)$$

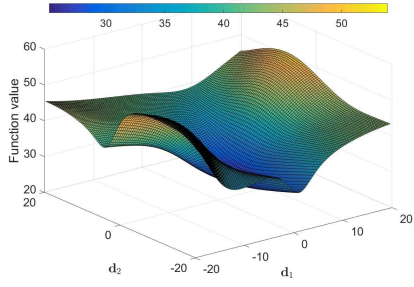
where \mathbf{t}_k^i is the k th sample of the input data, \mathbf{t}_k^o is the k th sample of the output data and $\hat{\mathbf{y}}$ is the neural network model, as a function of the input data and the model parameters, \mathbf{x} . We substitute Equation (8) into Equation (1) to obtain:

$$L(\mathbf{x}) = \frac{1}{2|\mathcal{B}|} \sum_{k \in \mathcal{B}} (\mathbf{t}_k^o - \hat{\mathbf{y}}(\mathbf{t}_k^i, \mathbf{x}))^2. \quad (9)$$

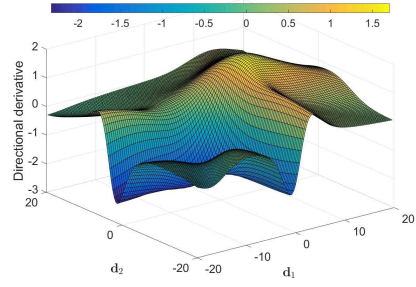
Therefore, the gradient of the loss becomes

$$\mathbf{g}(\mathbf{x}) = \frac{-1}{|\mathcal{B}|} \sum_{k \in \mathcal{B}} \nabla \hat{\mathbf{y}}(\mathbf{t}_k^i, \mathbf{x}) ((\mathbf{t}_k^o - \hat{\mathbf{y}}(\mathbf{t}_k^i, \mathbf{x}))), \quad (10)$$

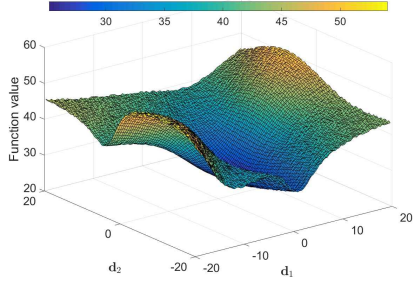
²Note that for consistency between the computed function values and gradient vectors, the same mini-batch is used when computing the function and gradient vector for a given weight vector \mathbf{x}



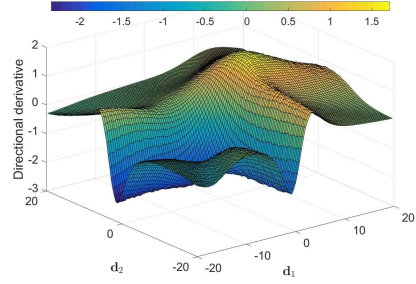
(a) Function value, $|\mathcal{M}| = 150$



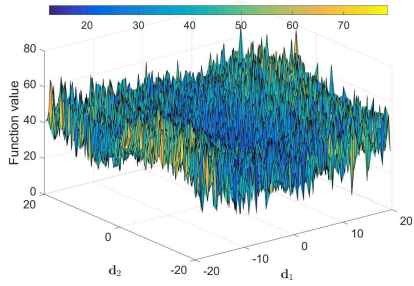
(b) Directional derivative, $|\mathcal{M}| = 150$



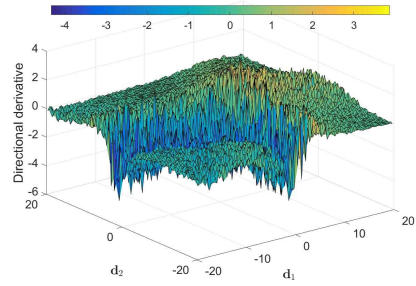
(c) Function value, $|\mathcal{B}| = 149$



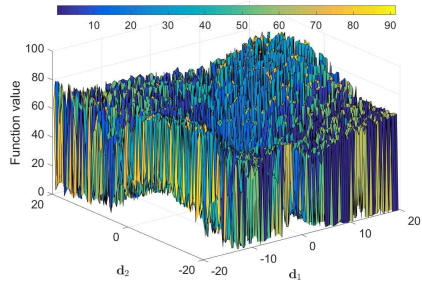
(d) Directional derivative, $|\mathcal{B}| = 149$



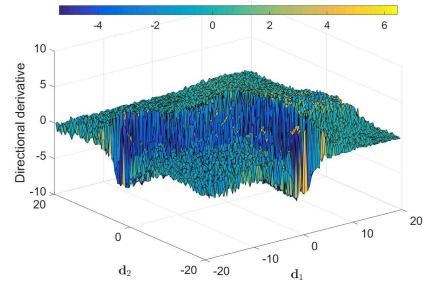
(e) Function value, $|\mathcal{B}| = 10$



(f) Directional derivative, $|\mathcal{B}| = 10$



(g) Function value, $|\mathcal{B}| = 1$



(h) Directional derivative, $|\mathcal{B}| = 1$

Figure 2: (a,c,e,g) Function value and (b,d,f,h) directional derivative plots along two random directions using batch sizes $\mathcal{B} \in \{150, 149, 10, 1\}$. Variance for both function and directional derivatives increases with decrease in batch size. It is evident that the directional derivative is affected less than the function values.

where the gradient of the model in terms of the model parameters is given by $\nabla \hat{\mathbf{y}}(\mathbf{t}_k^i, \mathbf{x})$. To aid understanding of the different contributing factors, consider the notation $A_k = (\mathbf{t}_k^o - \hat{\mathbf{y}}(\mathbf{t}_k^i, \mathbf{x}))$, which constitutes the prediction error term, and $\mathbf{C}_k = \nabla \hat{\mathbf{y}}(\mathbf{t}_k^i, \mathbf{x})$, which is the gradient of the model. This simplifies Equations (9) and (10) to

$$L(\mathbf{x}) = \frac{1}{2|\mathcal{B}|} \sum_{k \in \mathcal{B}} (A_k)^2, \quad (11)$$

and

$$\mathbf{g}(\mathbf{x}) = \frac{-1}{|\mathcal{B}|} \sum_{k \in \mathcal{B}} (\mathbf{C}_k A_k). \quad (12)$$

The product of $\mathbf{C}_k A_k$ determines the loss function gradient. In the loss function, Equation 11 depends only on the A_k term. According to the chain rule, the gradient of the model, \mathbf{C}_k , is a function of the weights and the derivatives of the activation functions, of the various layers in a neural network [Werbos, 1982]. For most activation functions, the derivative remains bounded. In our case, all the activation functions considered in this paper have derivatives ≤ 1 . This means that for a fixed batch, \mathcal{B} and a fixed point \mathbf{x} in space, which apply to both A_k and \mathbf{C}_k terms, the activation function derivatives are not going to increase the magnitude of information passing through the network.

Let us now consider a fixed point in space, \mathbf{x} , where we sample many mini-batches for a constant batch size $|\mathcal{B}| < M$. In this case both A_k and \mathbf{C}_k vary only as a function of \mathbf{t}_k , which we can express as expected values \bar{A}_k and $\bar{\mathbf{C}}_k$; with corresponding variance $\sigma(A_k)$ and $\sigma(\mathbf{C}_k)$ to obtain

$$L(\mathbf{x}) = \frac{1}{2|\mathcal{B}|} \sum_{k \in \mathcal{B}} (\bar{A}_k + \sigma(A_k))^2 = \frac{1}{2|\mathcal{B}|} \sum_{k \in \mathcal{B}} (\bar{A}_k^2 + 2\bar{A}_k\sigma(A_k) + \sigma(A_k)^2), \quad (13)$$

and

$$\begin{aligned} \mathbf{g}(\mathbf{x}) &= \frac{-1}{|\mathcal{B}|} \sum_{k \in \mathcal{B}} (\bar{\mathbf{C}}_k + \sigma(\mathbf{C}_k)) (\bar{A}_k + \sigma(A_k)) \\ &= \frac{-1}{|\mathcal{B}|} \sum_{k \in \mathcal{B}} (\bar{\mathbf{C}}_k \bar{A}_k + \sigma(\mathbf{C}_k) \bar{A}_k + \bar{\mathbf{C}}_k \sigma(A_k) + \sigma(\mathbf{C}_k) \sigma(A_k)). \end{aligned} \quad (14)$$

Hence, the variance in $L(\mathbf{x})$ is dictated by $2\bar{A}_k\sigma(A_k) + \sigma(A_k)^2$, while the variance in $\mathbf{g}(\mathbf{x})$ is dictated by $\sigma(\mathbf{C}_k)\bar{A}_k + \bar{\mathbf{C}}_k\sigma(A_k) + \sigma(\mathbf{C}_k)\sigma(A_k)$. Depending on \mathbf{x} , the variance $\sigma(A_k) \gg 1$ due to changes in the mini-batch, implies that the variance in $L(\mathbf{x})$ will be larger than the variance in $\mathbf{g}(\mathbf{x})$. This is due to the term $\sigma(A_k)^2$ dominating in Equation (13), while Equation (14) scales linearly in both $\sigma(A_k)$ and $\sigma(\mathbf{C}_k)$ which is bounded $\sigma(\mathbf{C}_k) \leq 1$, depending on \mathbf{x} .

Alternatively, the variance in $L(\mathbf{x})$ is significantly reduced when $\sigma(A_k) \ll 1$, since $\sigma(A_k)^2 \approx 0$, while $2\bar{A}_k\sigma(A_k)$ depends on the magnitude of \bar{A}_k . In turn, the variance in $\mathbf{g}(\mathbf{x})$ depends mainly on $\sigma(\mathbf{C}_k)$ which scales \bar{A}_k and $\sigma(A_k)$, while $\bar{\mathbf{C}}_k\sigma(A_k)$ also contributes. However, since $\bar{\mathbf{C}}_k \leq 1$ and $\sigma(\mathbf{C}_k) \leq 1$, the variance in $\mathbf{g}(\mathbf{x})$ is bounded. Hence, when $\sigma(A_k) \ll 1$ the variance in $\mathbf{g}(\mathbf{x})$ can be larger than $L(\mathbf{x})$. Also, when the magnitude of $\bar{A}_k \ll 1$ the variance in $L(\mathbf{x})$ is reduced as is evident in Figures 2(e,g). Lastly, it is evident that when $\bar{\mathbf{C}}_k \approx 0$, implying saturation of the activation function then the variance $\sigma(\mathbf{C}_k) \approx 0$, which in turn results in the variance of $\mathbf{g}(\mathbf{x})$ to diminish. The flat, low variance areas at the extremes of the sampled domains are particularly evident in the gradients sampled with small batches in Figure 2(f,h). These are examples of where the saturation of the activation functions drives down the variance in the gradient.

3.1 Mean and variance surface visualization

We now aim to qualify and quantify the influence of the variances of the function and directional derivative surfaces by conducting the following analysis. We explicitly evaluate and plot the mean of the function value and directional derivative surfaces in green, while the variance surfaces are plotted as blue. The mean and variance estimates were calculated using 50 independent draws of $\mathcal{B} = 10$ samples at every one of the 100x100 grid points. The full batch function value surface is also shown in red, see Figure 3(a).

This allows for the comparison between the full batch surface (red) and the estimated mean (green). If the estimated mean (green) dips below the full batch (red) surface,

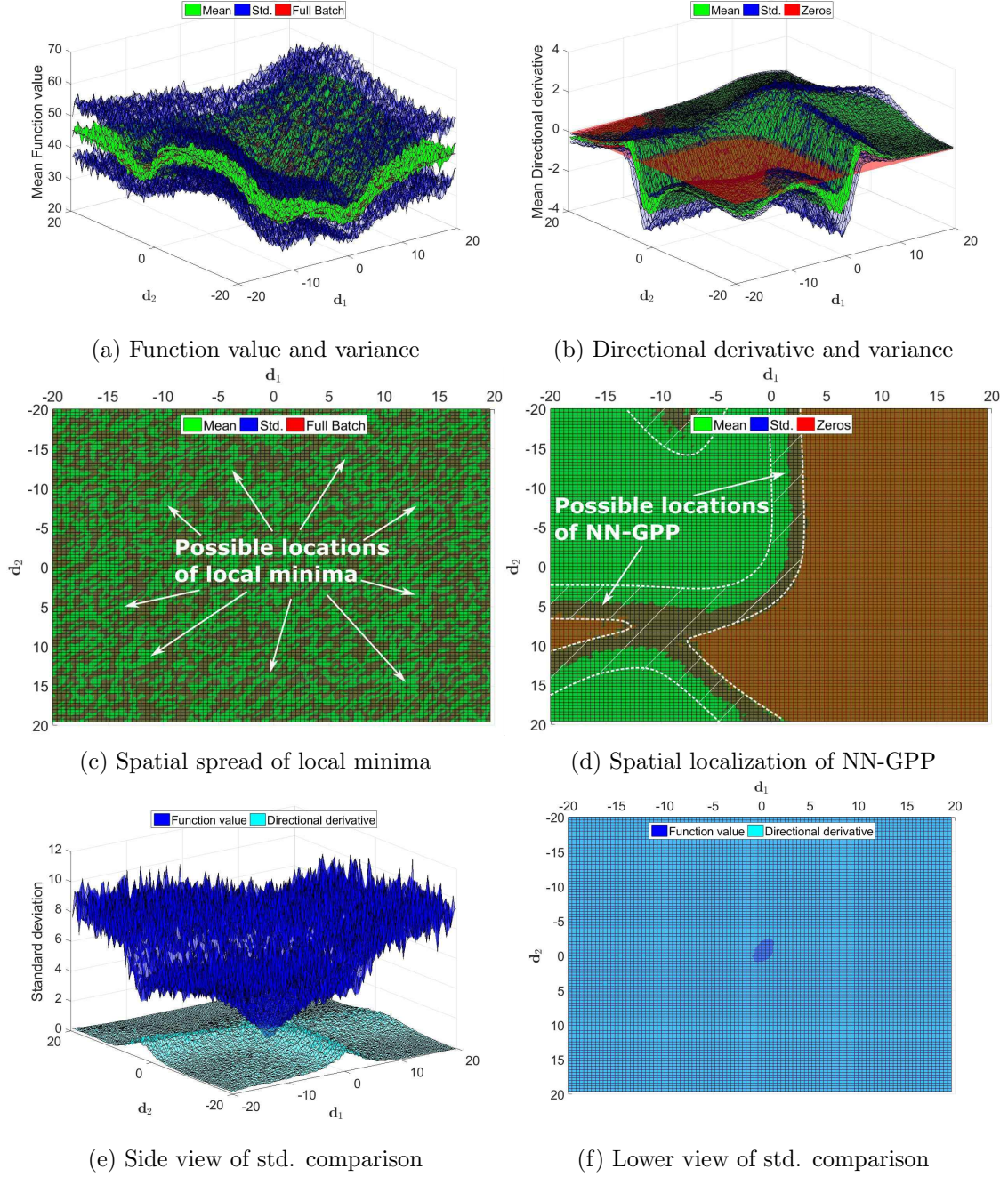


Figure 3: The Sigmoid activation function: Mean and standard deviation plots of (a) the loss and (b) directional derivatives. The estimates were calculated using 50 samples of batch size $|\mathcal{B}| = 10$ at every point of the 100 by 100 grid. In (a) the full batch loss is given in red, while in (b) the red plane denotes the zero directional derivative plane, indicating locations of sign changes. Viewing these plots from below (c,d) illustrate the spatial spread of potential optima in both function value and gradient-only paradigms. Instances where the mean dips below the full batch loss (green areas) in (c) denote potential local minima. In (d) the green regions denote negative and red areas positive directional derivatives respectively. The shaded contours in (d) are areas of uncertainty, where the variance protrudes through the zero plane, but the mean does not. The uncertainty bounds (one standard deviation) are indicated in white. The spatial spread of NN-GPPs is highly localized, while the function value minima are spread uniformly across the sampled domain. If we isolate the standard deviation of the (d) loss and (f) directional derivative, we observe a practical realization of the discussion in Section 3.

given the high variance, it is likely that a local minimum may occur at the given location. Conversely, if the estimated mean (green) lies above the full batch (red) surface, a spurious maximum is more likely to occur.

We therefore show the function value plot from below in Figure 3(c), such that areas, where the estimated mean (green) surface permeate through the full batch (red) surface, can be easily identified. The result is a uniformly distributed mixture of red and green, indicating that local minima are spread over the entire sampled surface. This highlights the challenges that a direct minimization strategy would face.

Considering the directional derivative plot in Figures 3(b) and (d), we are concerned with sign changes, when dealing with NN-GPP. Hence, we plot the zero plane in red, as a NN-GPP point would manifest when variance due to mini-batch sub-sampling causes sign changes in the directional derivative. This highlights the importance of not only considering the variance in the information (i.e. function values or directional derivatives) but also to what extent these variations manifest as apparent solutions to the problem. The latter is directly dependent on the optimality formulation under consideration. We show Figure 3(b) from below (i.e. the negative domain) in Figure 3(d), where negative directional derivatives are presented as green and positive directional derivatives as red. The shaded domains between these two regions are uncertainty areas, where the zero plane intersects the standard deviation, but not yet the mean. Since we only depict from below, the area of uncertainty is essentially double than what is indicated. The areas, where the probability of encountering a NN-GPP is high, are indicated in Figure 3(d). Immediately there is a stark contrast between Figures 3(c) and (d): The areas of possible NN-GPP occurrence are spatially localized, while the locations of possible local minima are almost uniformly distributed in the sampled domain. We remind the reader at this point, that both these plots represent the same loss function, yet the information gained from the plots is distinct, by using different optimization formulations. Defining the solution as a NN-GPP is more robust than minimizing the loss function.

3.2 Mean and variance univariate function visualization

As a number of optimization approaches used in neural network training [Robbins and Monro, 1951, Nesterov, 1983, Duchi et al., 2011, Kingma and Ba, 2015] make use of 1D directional information, we subsequently consider the behavior of the loss function and directional derivative along 1D search directions. Towards this aim, we select four directions within the search domain to give a more holistic view of the behaviour of the loss function and directional derivatives along these selected search directions.

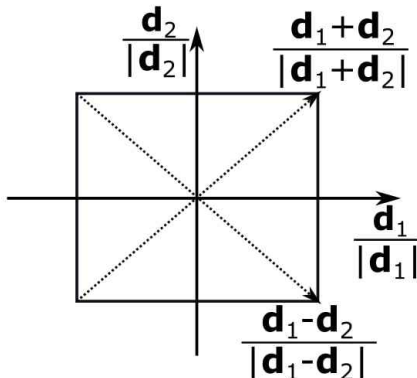


Figure 4: Diagram depicting the investigated 1D directions.

These chosen directions are the unit vectors along the uncoupled axes, $\frac{\mathbf{d}_1}{|\mathbf{d}_1|}$ and $\frac{\mathbf{d}_2}{|\mathbf{d}_2|}$, as well as the diagonals of the chosen axis directions, $\frac{\mathbf{d}_1+\mathbf{d}_2}{|\mathbf{d}_1+\mathbf{d}_2|}$, $\frac{\mathbf{d}_1-\mathbf{d}_2}{|\mathbf{d}_1-\mathbf{d}_2|}$, shown in Figure 4. We sample the function value and directional derivatives along these directions

and exhaustively count the number of local minimizers and NN-GPPs. The sum of the number of minima and NN-GPPs are given in the legend of the plots. The number indicated reflects the sum of the minimizers of NN-GPPs along all four directions. We also show histograms of the spatial distribution of the minimizers and NN-GPPs along the respective search directions.

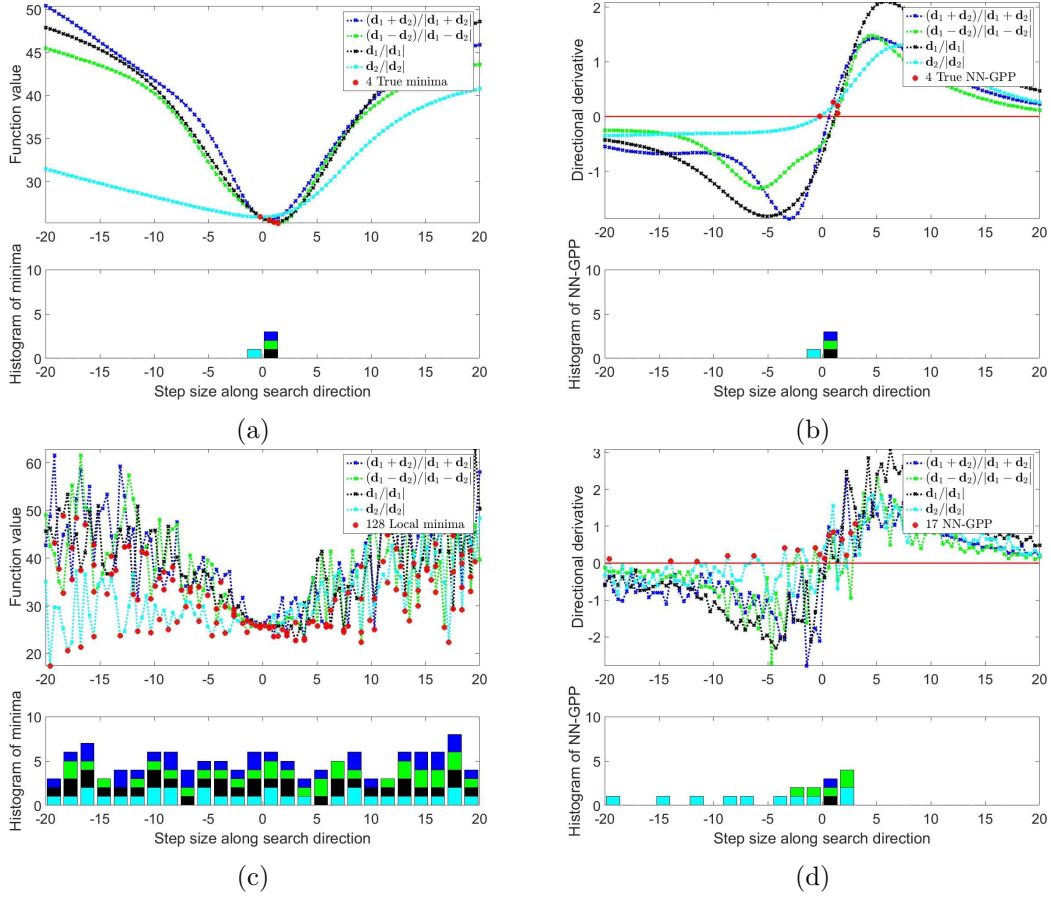


Figure 5: The Sigmoid activation function: 1-D plots of the (a) function value and (b) directional derivative along fixed directions of the 2-D domains. We compare two states, using full batches, $|\mathcal{M}| = 150$, and mini-batches, $|\mathcal{B}| = 10$. We explicitly count and record the number local minima and NN-GPP in either case according to the respective definitions. As in the 2-D case, the locations of the local minima are uniformly distributed along the sampled domains for all directions. In the case of the directional derivative, the spatial location is dependent on the direction being sampled. In directions that contain high curvature, such as \mathbf{d}_1 , the sign change is highly localized. In the case of \mathbf{d}_2 , some of its domain moves along the area of uncertainty in Figure 3, which makes the location of NN-GPP along this search direction more widespread in that area.

The sampled search directions using the Sigmoid activation function are shown in Figure 5. The true optima are indicated by the full batches in Figure 5(a) and (b), where we see equivalence between a local minimum and NN-GPP as the function and derivatives are continuous and smooth. Each search direction exhibits a single true minimum or true NN-GPP at exactly the same points along the search directions.

However, when using mini-batch sampling, both the loss and directional derivative functions are discontinuous, with a significant difference between minimizers and NN-GPPs. As is the case in the 2-D plots of Figure 3, the spatial distribution of local minima is spread uniformly along the search directions as is evident from Figure 5(c). In turn, the spatial distribution of NN-GPPs much more localized around the true NN-GPPs as shown in Figure 5(d). The direction with the highest variance is \mathbf{d}_2 , which is still half

the variance of the lowest minima distribution. The first half along \mathbf{d}_2 runs along an area of uncertainty for NN-GPP typical of Figure 3(d). Due to the low directional derivative value and the corresponding variance, it is possible to encounter spurious sign changes along this ridge. We included \mathbf{d}_2 to investigate the variance of NN-GPPs when it runs through uncertain areas. The remaining three directions are tightly clustered around the true NN-GPPs, indicating small spatial domains of uncertainty.

Subsequently, we extend our investigation to a number of popular activation functions, investigating their effect on finding minimizers and NN-GPPs as well as studying their spatial location.

4 Alternative Activation Functions

In the past, Sigmoid activations were popular, but subsequently other smooth activations, such as Tanh [Karlík, 2015] and Softsign [Bergstra et al., 2009], have been preferred. In line with work done by Xu et al. [2017], we call this the saturation class of activation functions. Today, the state of the art networks use activation functions which promote sparsity, namely the ReLU [Glorot and Bordes, 2011] family of activations. We include leaky ReLU [Maas et al., 2013] and ELU [Clevert et al., 2016] into this category and refer to this family as the sparsity class of activations. Both these classes are plotted in Figure 6 for comparison.

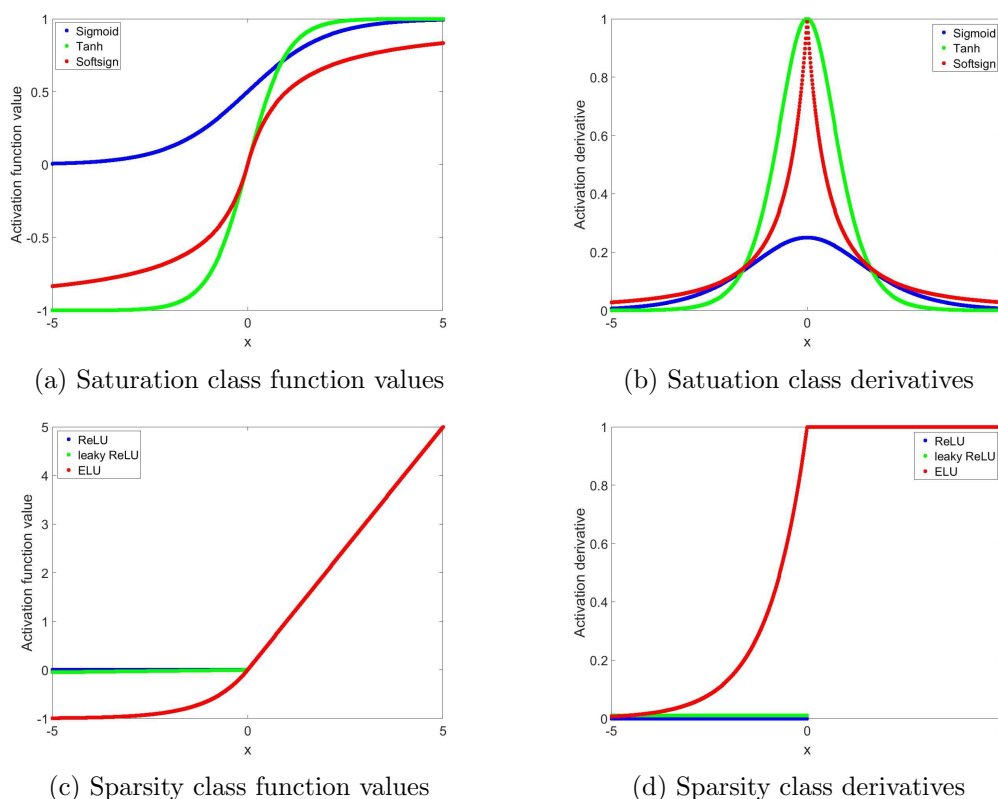


Figure 6: (a,c) Function value and (b,d) derivatives of activation functions considered in our investigations. These are lumped together into (a,b) saturation and (c,d) sparsity classes. The saturation class makes use of the non-linearities of the activation functions to construct mappings. The sparsity class makes use of the architecture in the network to introduce the non-linearities, where specific "channels" in the network are active or not, depending on weights and data.

As their name suggests, the dominant characteristic of the saturation class is the stagnating, plateau-like behavior at in both negative and positive extremes of the x-domains.

The differences within the saturation class concentrate primarily on the numerical ranges of these saturation points, as well as the curvature of their "active" domains, around 0. As we will demonstrate, the differences between the activation functions, though slight in their elemental form, can lead to significant changes in the loss function of a neural network where they are applied.

The sparsity class have fundamentally different characteristics to the saturation class in that they allow a linear relationship in their "activated" positive domain, while enforcing or approximating an "off" characteristic in the negative domain. The ReLU activation function enforces a "hard off", setting the function value and derivative to 0 for the negative x -domain. The leaky ReLU allows a small positive that is constant in the negative domain of x . The transition to the positive domain x is discontinuous in the derivative. The ELU formulation constructs the derivative to be smooth and continuous over the negative domain of x , while it transitions to a constant over the positive domain of x .

4.1 Activation function influence for random directions over large domains

We now investigate the effect of a number of popular activation functions (AFs) on the distribution of minimizers and NN-GPPs. This is done using exactly the same study as conducted with Sigmoids in Section 3, where the only change is the change of activation function. This allows for detailed comparison between AF results. The results are summarized in Table 1, while the detailed plots are given for completeness in Appendix A.

Concerning the histogram plots, since NN-GPP are determined as being after the sign change in our analyses, cases occur where the location of the true optimum is close to edge of a bin in the histogram. In such instances the location of the NN-GPP might be noted in a bin that is to the right of that indicated for the minima. This is not an error, but simply an artifact of how the minima and NN-GPP are identified from discrete samples of the loss function and directional derivative.

One of the prominent differences between the saturation and sparsity activation function classes is the behaviour on the extremities of the sampled domains. The saturation functions have "mountainous" features, in the sense that the landscape alternates between high and low curvature regions. This occurs as different nodes in the network saturate, or activate. When most but not all nodes have saturated, flat planes with low directional derivative values can be observed. This can have a negative effect on the spatial distribution of NN-GPPs. as seen in Figures 5(d), 7(h) and 8(h). In cases where saturation is high, the directional derivative magnitude is low. Hence, the variance of the directional derivative is lower than other areas of the loss function, but that small variances may create spurious NN-GPPs as the directional derivative magnitude is close to zero. This is particularly prevalent for the Tanh activation function, seen in Figure 7(h), which also has the fastest saturation rate, see Figure 6. Conversely, the NN-GPP are highly localized for the Softsign analysis, since the saturation occurs at a far slower rate, see Figures 6 and 8(h). This demonstrates that the derivative shape of the activation function matters with respect to finding minimizers as well as NN-GPPs.

The sparsity class exhibits very steep behavior at the outer limits of the domain. This is a feature coupled to the "on" nature of the activation functions. When most/all activations at the various network nodes are in the positive domain, the input data is passed through the network and potentially amplified by large weights. Since we implement the MSE loss for these examples, any classification error above 1 gets squared, resulting in the aggressive increase in error. The consequence of this is a relatively convex looking loss function. However, in the center of the domain, where the error is small, a significant amount of detail is present that is lost when considering the large scales used in the current analysis. It is also notable, that the number of true optima obtained in ReLU

A.F.	Figure	# True Optima	# Minima	# NN-GPP	Comments
Sigmoid	2, 5	4	128	17	Smooth features, spurious NN-GPP in low curvature directions.
Tanh	7	4	126	23	Higher curvature; NN-GPP more localized, but high saturation, leading to false NN-GPP at edges.
Softsign	8	4	117	5	More curvature than Sigmoid, less than Tanh; more curvature at origin gives better localization; less saturation at ends means less spurious NN-GPP.
ReLU	9	8	104	13	Exponential behaviour in MSE loss; Globally convex shape, but locally intricate; more true optima; no saturation, no spurious NN-GPP at edges.
Leaky ReLU	10	8	101	17	No different to ReLU at global scale; low curvature directions have more spurious NN-GPP due to leaky gradient (as opposed to hard-zero).
ELU	11	4	99	5	Less true optima than other ReLUs; smooth loss function features; higher gradient curvature, resulting in more localized NN-GPP.

Table 1: Summary of observations from analyses conducted with random directions and large (global) domains. The corresponding Figures 7-11 are included in Appendix A.

and leaky ReLU activation functions are different to the rest for the same problem. This is a clear indication, that there are unique features in the local domain that distinguish these activations from the rest. In search for these features, we conduct a second, more localized analysis in the next Section.

However, the most important aspect of this investigation is that the behavior of the optimality formulations explored in Section 3 hold across all activation functions. The number of local minima is often around an order of magnitude more than the equivalent number of NN-GPP. The local minima are spatially spread across the whole domain, whereas only low curvature directions exhibit a high number of spurious NN-GPP. This aligns well with overarching trends in optimization which prefer high curvature directions, as is evident with the emphasis on second order methods in mathematical programming [Arora, 2011] and the corresponding efforts to include them into machine learning [Schraudolph et al., 2007, Martens, 2010].

5 A closer look at descent directions

In this section we modify the definitions of \mathbf{d}_1 and \mathbf{d}_2 , to be the steepest descent direction of the full batch, $\mathbf{d}_1 = -\nabla\mathcal{L}(\mathbf{x})$ at initial starting point \mathbf{x}_0 located at $(0,0)$, and \mathbf{d}_2 is chosen to be a random direction approximately perpendicular to \mathbf{d}_1 . We also reduce the grid range to $[-2,2]$, to give a more detailed perspective of characteristics around local minima. A summary of the observations made is given in Table 2.

The most prominent feature of the ReLU loss function is that it does not have uniform

A.F.	Figure	# True Optima	# Minima	# NN-GPP	Comments
Sigmoid	12	4	117	37	Smooth features, spurious NN-GPP again in low curvature directions, mainly the contour direction.
Tanh	13	4	130	12	Higher curvature than Sigmoid; NN-GPP fewer more localized, contour direction generates spurious NN-GPP over whole domain.
Softsign	14	4	123	11	More local curvature than Tanh; NN-GPP highly localized.
ReLU	15, 17	5	105	26	Piece-wise; multi-modal with shallow basins; directional derivatives are discontinuous; existence of flat planes when all nodes are "off" (insensitive to sub-sampling); quadratic when all nodes are "on"
Leaky ReLU	16, 17	5	124	28	Similar features to ReLU, but "flat planes" have slight curvature
ELU	18	4	121	16	Smooth loss function features; uni-modal in diagonal directions; continuous directional derivative; higher gradient curvature; most localized NN-GPP for ReLUs.

Table 2: Summary of observations from analyses conducted on smaller (local) domains, with corresponding Figures 12-18 shown in Appendix B. Here the search directions are $\mathbf{d}_1 = -\nabla\mathcal{L}(\mathbf{x})$ and \mathbf{d}_2 is a random perpendicular direction to \mathbf{d}_1 .

characteristics. There are flat planes, low curvature optima, high curvature optima, and quadratic characteristics almost seemingly stitched together as is evident in Figure 15(a). There are up to two optima in a given search direction. These optima are separated, some are in very shallow basins (in the negative domains) and others are in basins of higher curvature (around 0.5 units). This "stitched" behavior in the loss function corresponds to the discontinuous nature of the directional derivative, seen in Figure 15(b). Here, the steps indicate different nodes switching "on" and "off". This is in stark contrast to other activation functions, which have smooth transitions between the activation and deactivation of nodes. The less nodes are active, the less curvature is present in the loss function. This explains the multiple optima with different curvature characteristics. If many nodes are on simultaneously with high weight values, the classification error increases and the loss function increases quadratically.

Importantly, there are also domains in the ReLU loss function where the directional derivatives are exactly 0. These are domains where all nodes are "off" and no information is able to pass through the network. These areas are unaffected by mini-batch sub-sampling, returning directional derivatives that are consistently 0. This is due to the magnitude of the weights in the network pushing the incoming data so far into the negative domain of the ReLU activation function, that all of the sample variance is in the negative domain. These are problematic areas for neural network training, since most training algorithms make use of gradient information to update \mathbf{x} . If there is no gradient information, there will be no updates to the state of the network and training comes to a premature halt. These flat planes are also present for the leaky ReLU. However, for leaky ReLU these do not have 0 derivatives (see Figure 17), thus preventing

training algorithms from being stranded during optimization. The additional curvature and smooth transition of gradients given by the ELU activation function further aid in constructing smooth features in the loss function. In this analysis these characteristics have led to a lower number of local optima, and have further aided the location of NN-GPP in the mini-batch setting (see Figure 18).

For this analysis we see the same trends in the sub-sampled loss functions: High curvature directions contain lower numbers of spurious NN-GPP, which are also more localized. Low curvature directions result in a wider range of possible NN-GPP locations and in some cases can even cause the likely location of NN-GPP to shift slightly. Specifically, the close-up Softsign analysis shows the disappearance of a NN-GPP out of the edge of the sampled domain. The true NN-GPP at the very beginning of the domain moves beyond $[-2,2]$ to fall between $[-3.5,-3.1]$ (confirmed by multiple mini-batch analyses in this extended domain). This NN-GPP is far from the true NN-GPP. If an optimization method were to find the solution in the $[-3.5,-3.1]$ range, it would be a bad representation of the true NN-GPP. This underlines the argument of preferring directions of high curvature for optimization purposes.

Overall, the same general trend holds for investigations on both the global and local domains conducted in this paper: Across all activation functions high curvature directions are beneficial for robust identification of NN-GPP in mini-batch sub-sampling. Searching for minimizers yields non-localized candidate optima with an order of magnitude higher occurrence than NN-GPP. The activation functions that produced the best results for finding NN-GPPs were Softsign and ELU for their respective classes, due to their favorable derivative characteristics.

6 Conclusion

This paper visually explores the local minimum and Non-Negative Associated Gradient Projection Point (NN-GPP) definitions in the context of sub-sampled neural network loss functions with different activation functions. We investigate the ability of apparent function minimizers and apparent NN-GPPs to localize the true (full batch) optimum when only mini-batches are computed. Function minimizers formulated as the standard mathematical programming problem give rise to a large number of spurious apparent minima, which are high in number and spatially distributed with large variance around true full batch minimum. Even, worse the apparent local minima are essentially uniformly distributed throughout the domain. This will hinder most attempts to incorporate line searches into neural network training.

NN-GPPs, formulated as the solution to the gradient-only optimization problem, result in apparent NN-GPP that are on average an order of magnitude less in number than the equivalent local minima over the same domain. Importantly, the spatial distribution of these NN-GPPs are bounded and concentrated around the true NN-GPP, or equivalently local minimum, since the full batch function is smooth. The spatial variance of the NN-GPPs depend on the curvature in the loss function along the search direction. High curvature tends to result in spatially concentrated NN-GPP, while low curvature search directions result in larger areas of uncertainty.

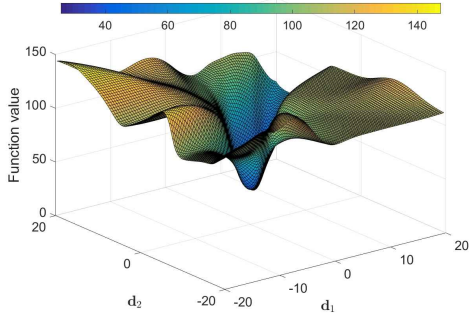
The curvature of the loss function is sensitive on the activation function chosen in the neural network. Therefore it is of interest to choose activation functions that aid in constructing high curvature search directions, while avoiding characteristics that might lead to the construction of numerous local optima, or flat planes with zero derivatives. We divide the investigated activation functions into two classes, namely: The saturation and sparsity. These classes have different characteristics and therefore can be used in distinct contexts. According to our investigations, the activation functions for each class with the most favorable characteristics for locating high quality NN-GPP in stochastic loss functions were Softsign and ELU respectively. The ability to find optima more

reliably in stochastic loss functions is critical to constructing better optimizers. Neural network models in particular can benefit from considering training as finding NN-GPP as opposed to only minimizing the loss function. This revision may aid in the construction of methods to solve efficient, automated neural network training, which is still an open problem.

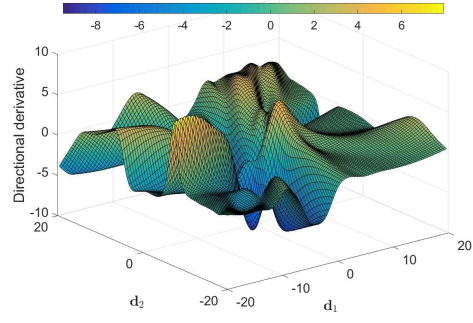
Acknowledgements

This work was supported by the Centre for Asset and Integrity Management (C-AIM), Department of Mechanical and Aeronautical Engineering, University of Pretoria, Pretoria, South Africa.

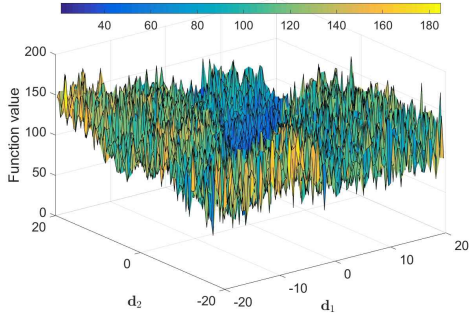
Appendix A.



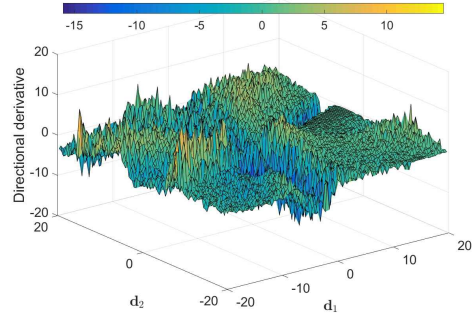
(a) Function value, $|\mathcal{M}| = 150$



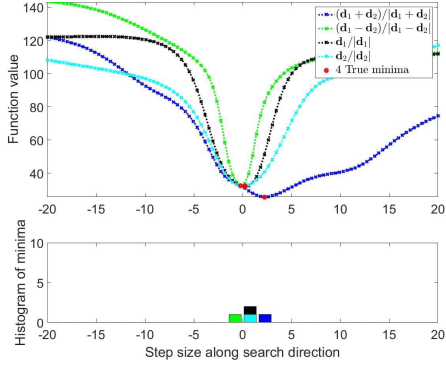
(b) Directional derivative, $|\mathcal{M}| = 150$



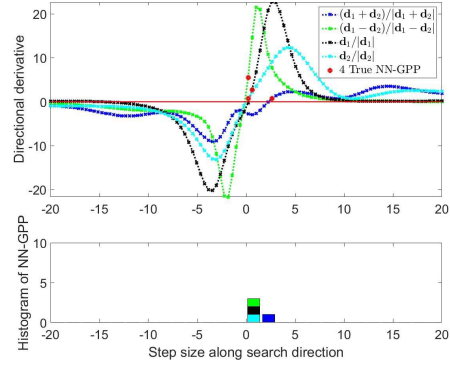
(c) Function value, $|\mathcal{B}| = 10$



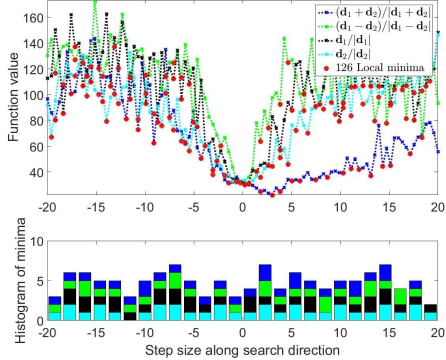
(d) Directional derivative, $|\mathcal{B}| = 10$



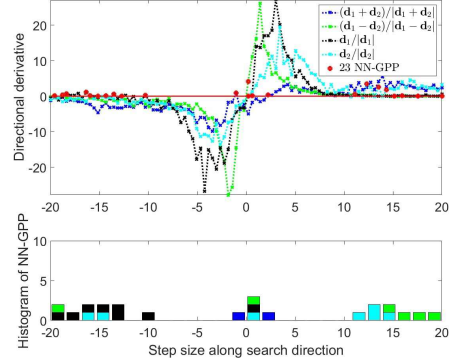
(e) True minima along search directions



(f) True NN-GPP along search directions

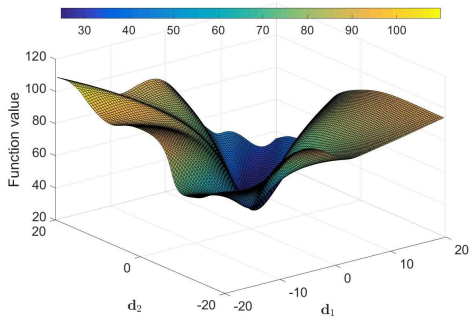


(g) Local minima along search directions

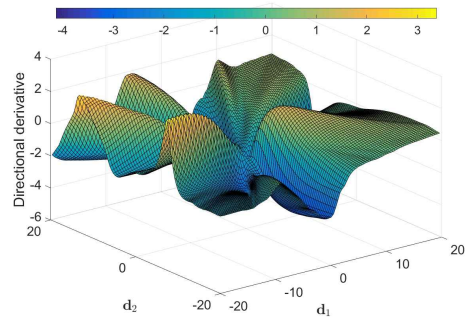


(h) NN-GPP along search directions

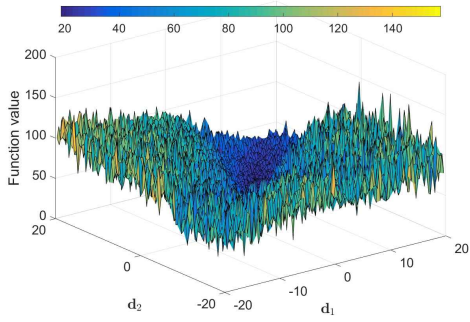
Figure 7: The Tanh activation function: A steeper AF derivative around 0 means more curvature in the loss gradients, which manifest as steeper directional derivatives. This aids NN-GPP localization in the active region (origin of (h)), but not at saturation (outer ranges of (h)).



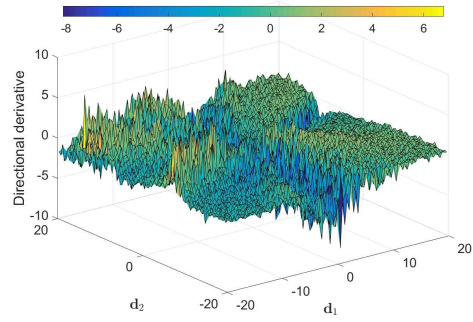
(a) Function value, $|\mathcal{M}| = 150$



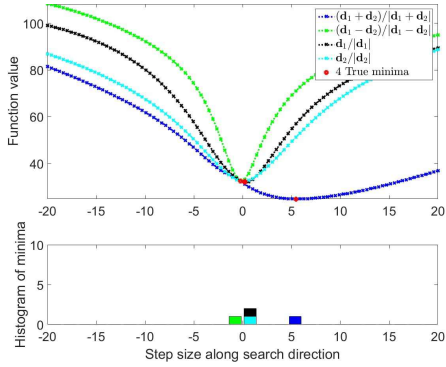
(b) Directional derivative, $|\mathcal{M}| = 150$



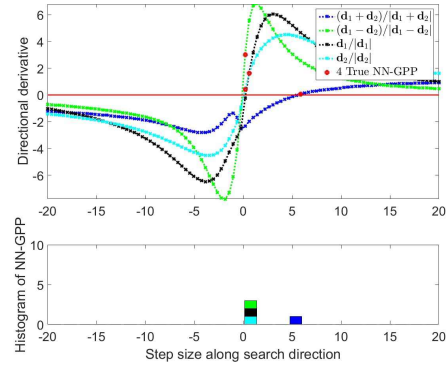
(c) Function value, $|\mathcal{B}| = 10$



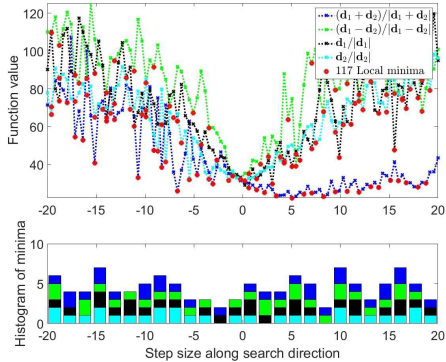
(d) Directional derivative, $|\mathcal{B}| = 10$



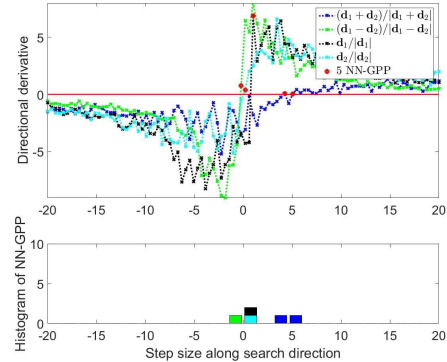
(e) True minima along search directions



(f) True NN-GPP along search directions

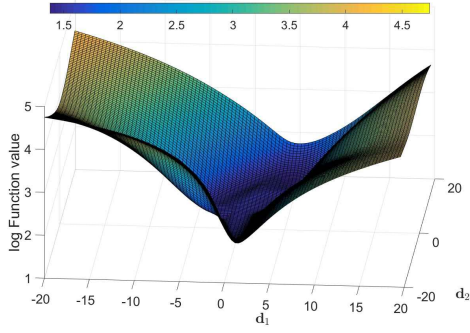


(g) Local minima along search directions

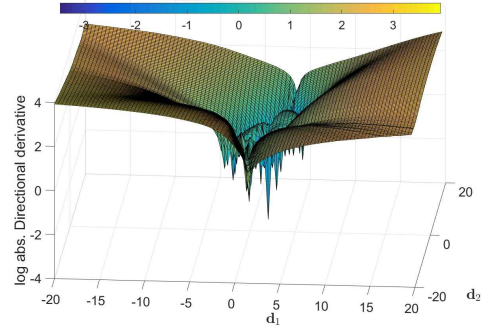


(h) NN-GPP along search directions

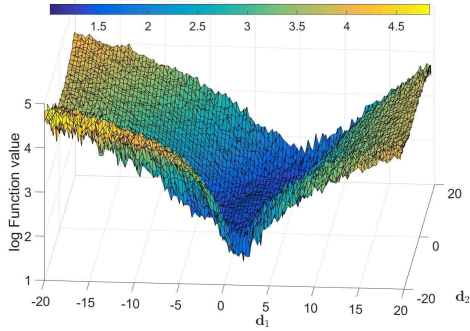
Figure 8: The Softsign activation function: The less aggressive taper-off in the AF derivative reduces the chance for spurious NN-GPP in the saturation regions. NN-GPPs during mini-batch sub-sampling are highly localized around the full batch true NN-GPPs.



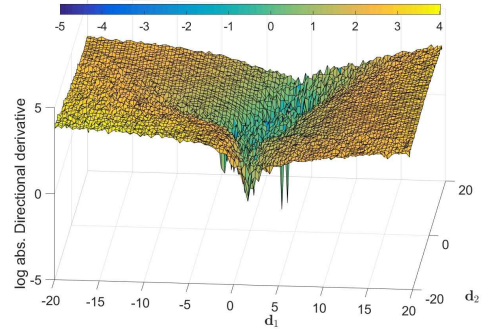
(a) Function value, $|\mathcal{M}| = 150$



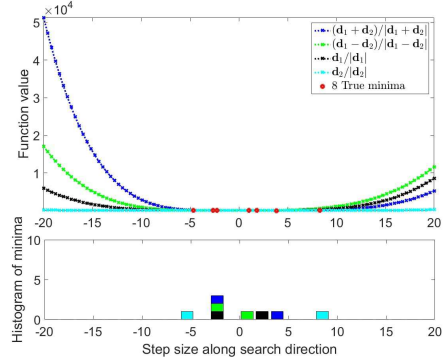
(b) Directional derivative, $|\mathcal{M}| = 150$



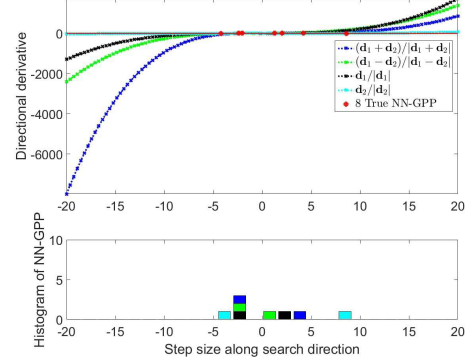
(c) Directional derivative, $|\mathcal{B}| = 10$



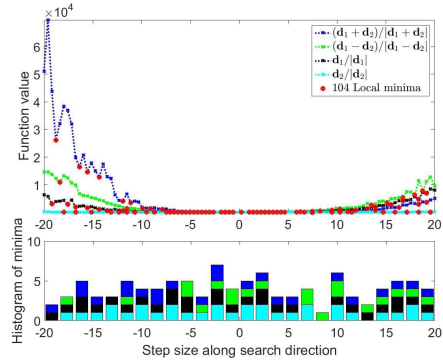
(d) Function value, $|\mathcal{B}| = 10$



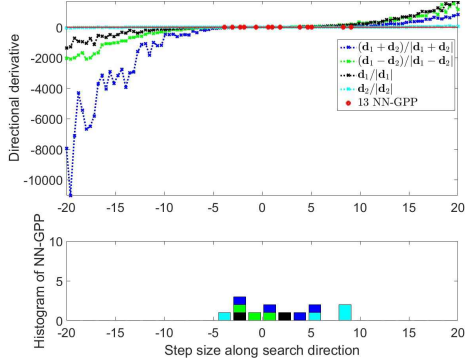
(e) True minima along search directions



(f) True NN-GPP along search directions

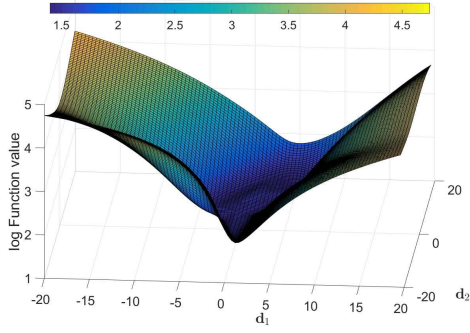


(g) Local minima along search directions

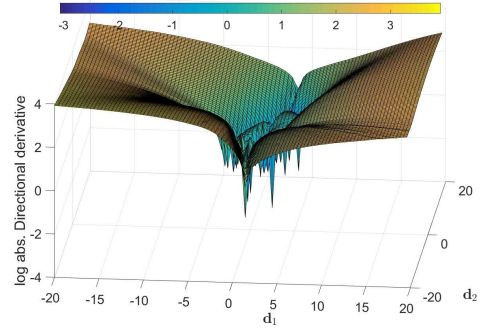


(h) NN-GPP along search directions

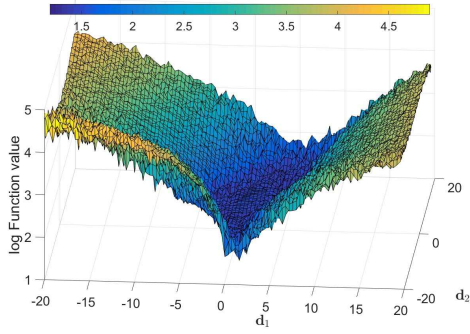
Figure 9: The ReLU activation function: Pushing ReLU activations far into their active domain results in convex behavior of the MSE loss function on a large scale. However, directional derivative and true optima plots indicate that more detail is contained in the basin.



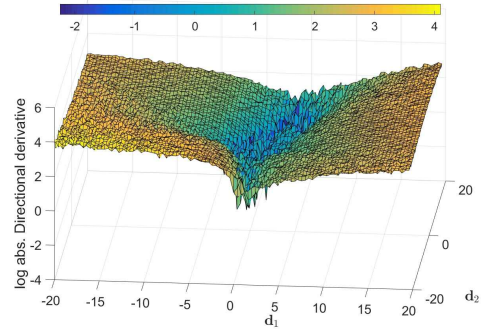
(a) Function value, $|\mathcal{M}| = 150$



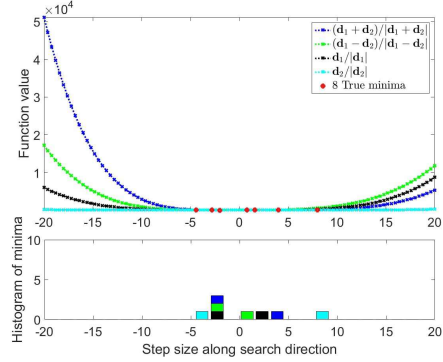
(b) Directional derivative, $|\mathcal{M}| = 150$



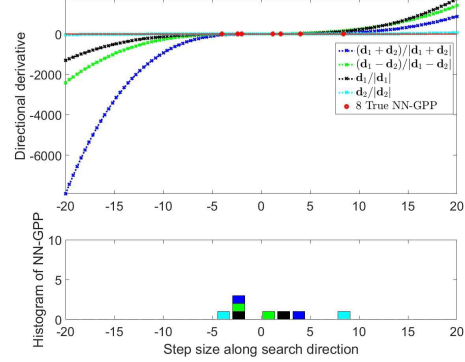
(c) Function value, $|\mathcal{B}| = 10$



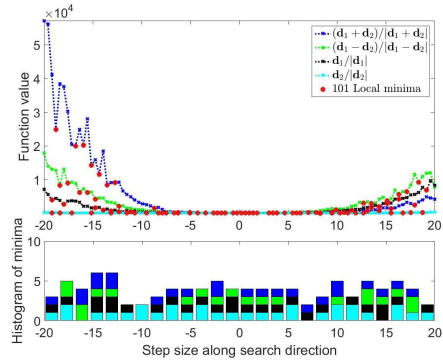
(d) Directional derivative, $|\mathcal{B}| = 10$



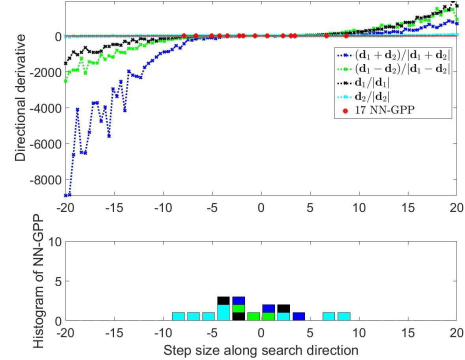
(e) True minima along search directions



(f) True NN-GPP along search directions

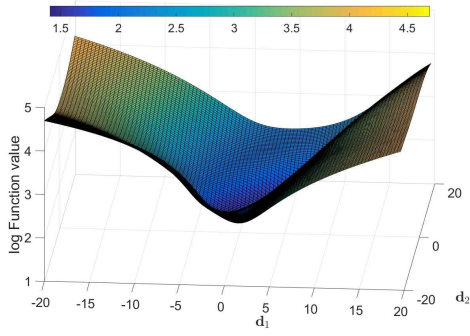


(g) Local minima along search directions

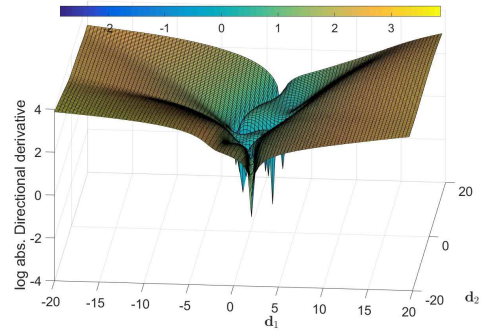


(h) NN-GPP along search directions

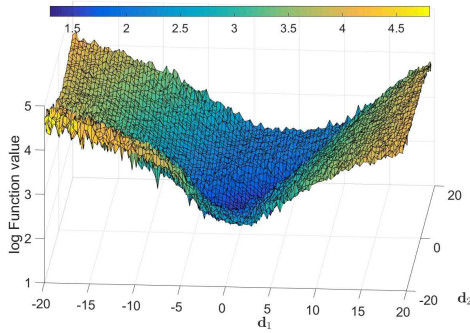
Figure 10: The leaky ReLU activation function: Since the magnitude of the "leaky" gradient is relatively small, its contribution is not apparent at this length scale. Therefore, the plots look very similar to those of ReLU. NN-GPPs are concentrated around the center, where the magnitude of the directional derivatives is small.



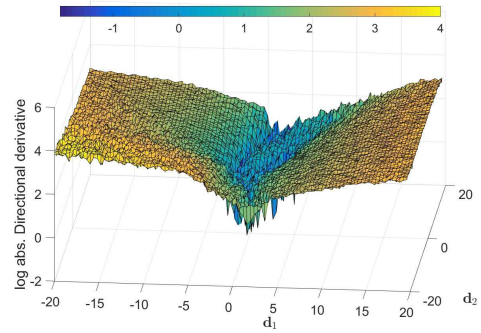
(a) Function value, $|\mathcal{M}| = 150$



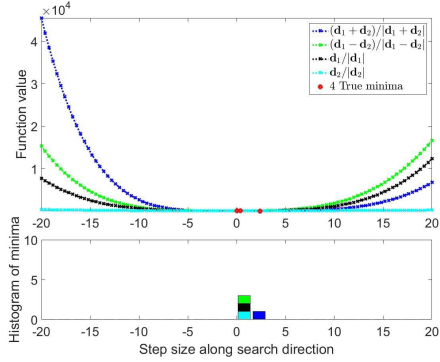
(b) Directional derivative, $|\mathcal{M}| = 150$



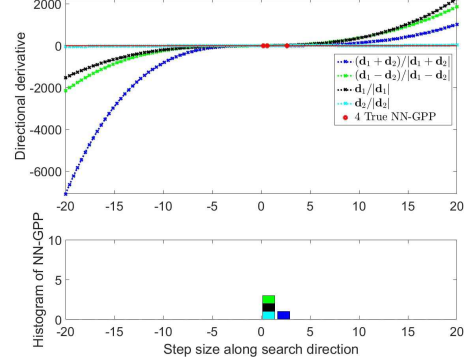
(c) Function value, $|\mathcal{B}| = 10$



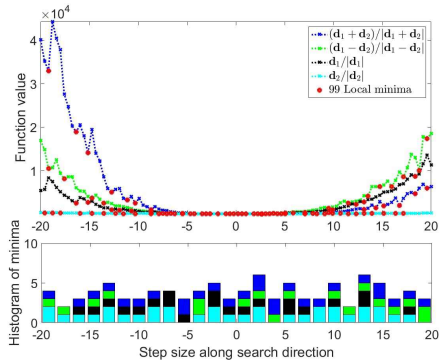
(d) Directional derivative, $|\mathcal{B}| = 10$



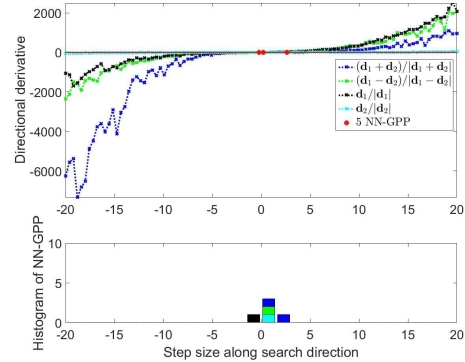
(e) True minima along search directions



(f) True NN-GPP along search directions



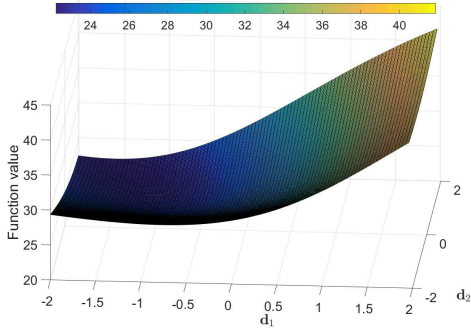
(g) Local minima along search directions



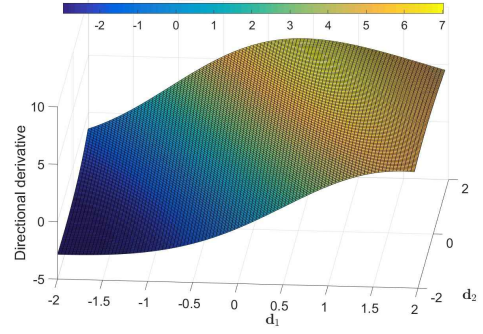
(h) NN-GPP along search directions

Figure 11: The ELU activation function: The shapes of the convex element of the loss function are similar to those of the other ReLUs. However, the structure in the basin seems to be different. This is confirmed by the number of true minima and NN-GPPs. The narrow spatial grouping of NN-GPPs is the contribution of the continuous derivative.

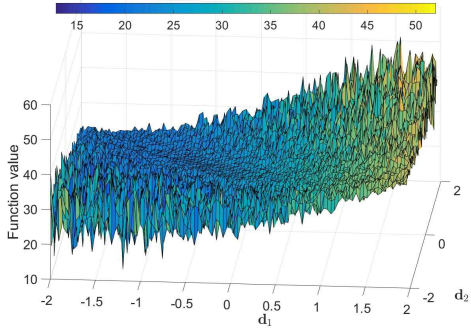
Appendix B.



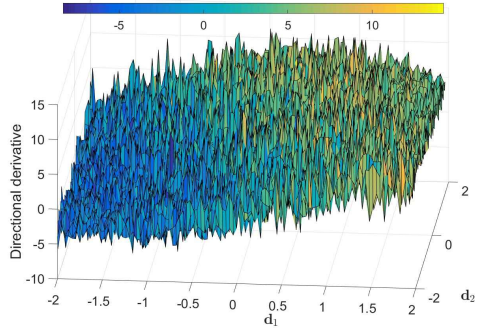
(a) Function value, $|\mathcal{M}| = 150$



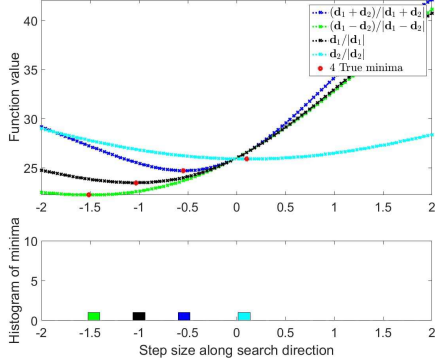
(b) Directional derivative, $|\mathcal{M}| = 150$



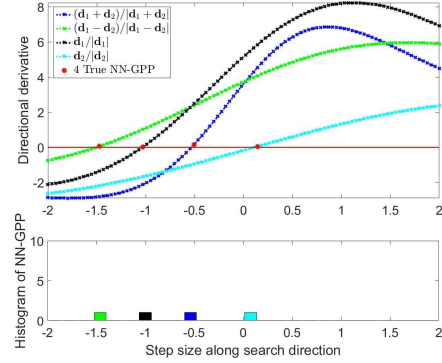
(c) Function value, $|\mathcal{B}| = 10$



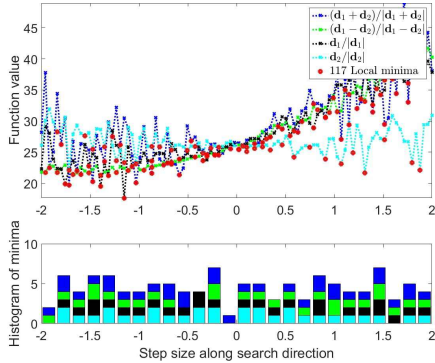
(d) Directional derivative, $|\mathcal{B}| = 10$



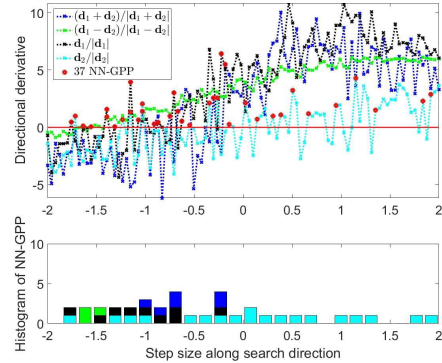
(e) True minima along search directions



(f) True NN-GPP along search directions

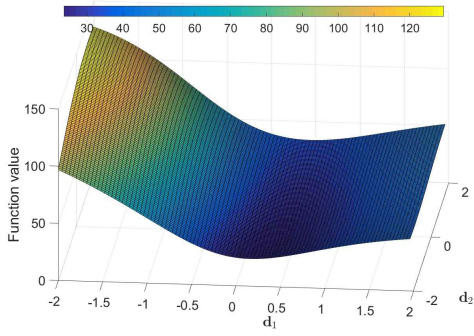


(g) Local minima along search directions

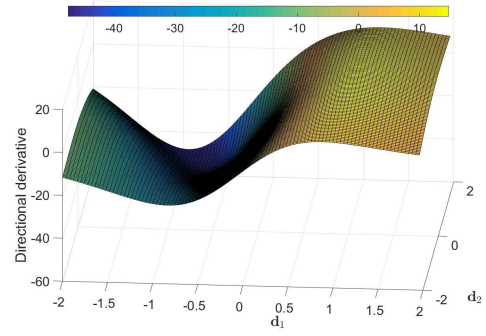


(h) NN-GPP along search directions

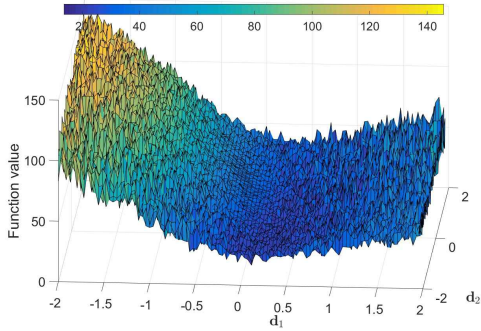
Figure 12: The Sigmoid activation function closeup: Shapes are smooth and have little curvature. NN-GPP have a smaller spatial range in directions where the curvature is larger, while being more spread out in low curvature directions.



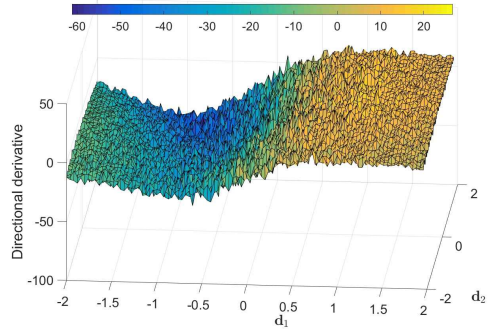
(a) Function value, $|\mathcal{M}| = 150$



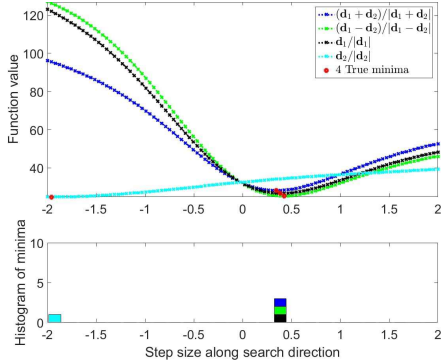
(b) Directional derivative, $|\mathcal{M}| = 150$



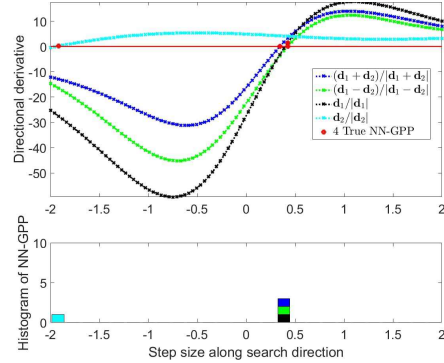
(c) Function value, $|\mathcal{B}| = 10$



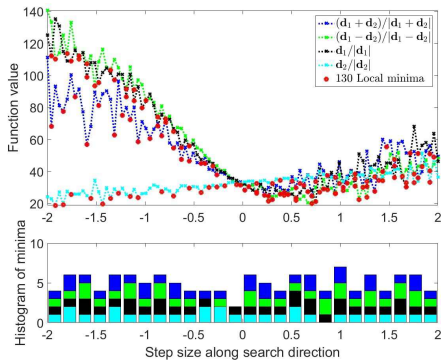
(d) Directional derivative, $|\mathcal{B}| = 10$



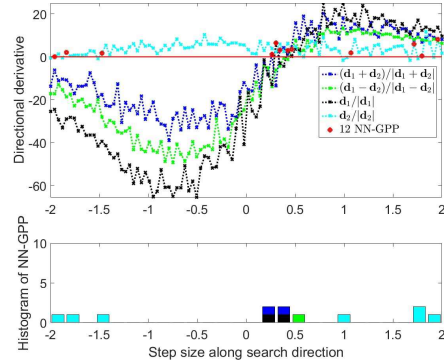
(e) True minima along search directions



(f) True NN-GPP along search directions

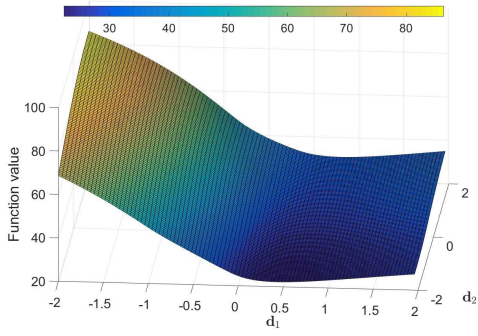


(g) Local minima along search directions

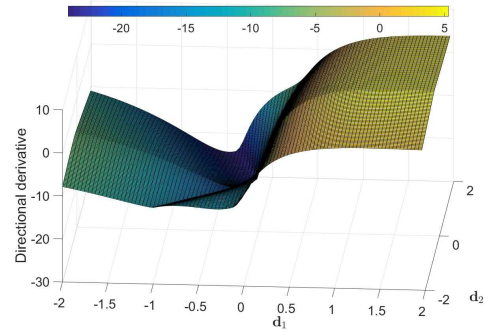


(h) NN-GPP along search directions

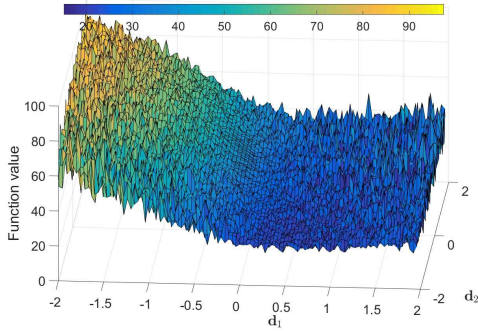
Figure 13: The Tanh activation function closeup: The higher curvature of Tanh helps localize NN-GPPs. Though this example captures lower variance directions in the function value (see \mathbf{d}_2), this does not alleviate the problem of uniformly spread spurious local minima.



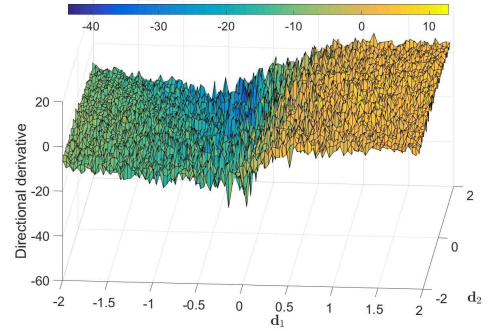
(a) Function value, $|\mathcal{M}| = 150$



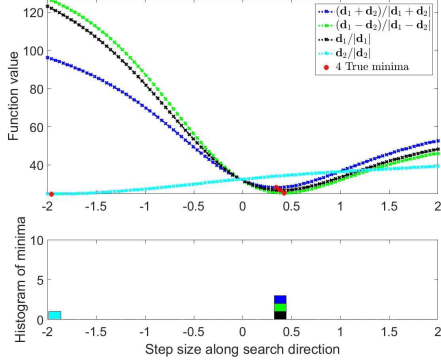
(b) Directional derivative, $|\mathcal{M}| = 150$



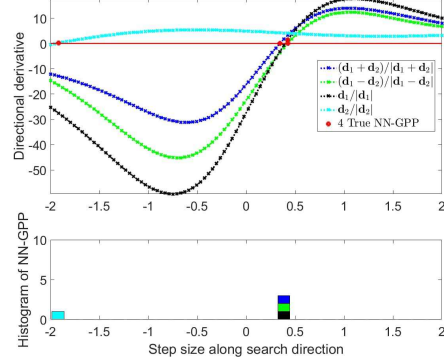
(c) Function value, $|\mathcal{B}| = 10$



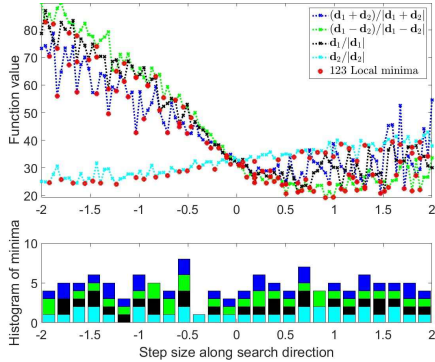
(d) Directional derivative, $|\mathcal{B}| = 10$



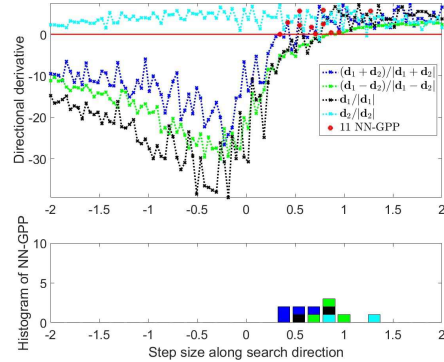
(e) True minima along search directions



(f) True NN-GPP along search directions

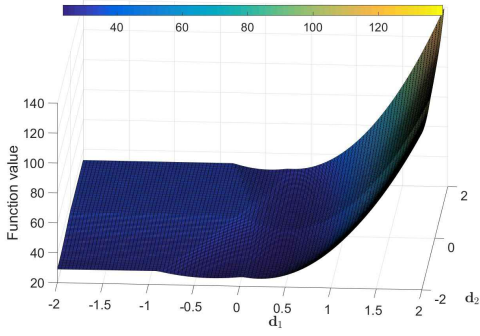


(g) Local minima along search directions

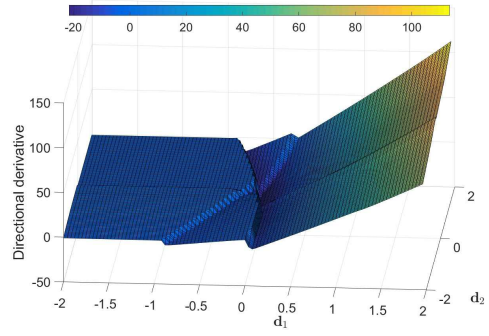


(h) NN-GPP along search directions

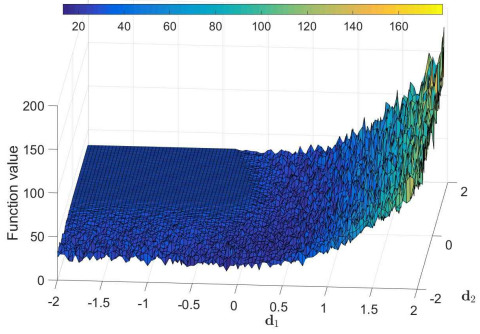
Figure 14: The Softsign activation function closeup: The small domain investigation confirms that the less aggressive taper-off of the AF derivative contributes to localizing mini-batch samples NN-GPPs around the true NN-GPP, while avoiding spurious instances at saturation. Local minima remain uniformly distributed.



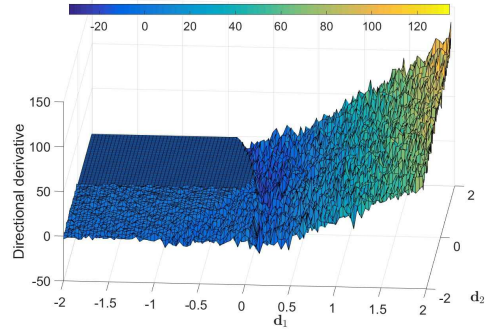
(a) Function value, $|\mathcal{M}| = 150$



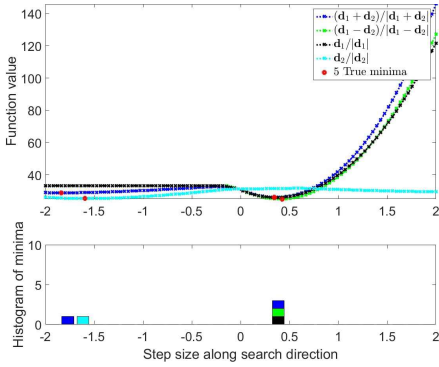
(b) Directional derivative, $|\mathcal{M}| = 150$



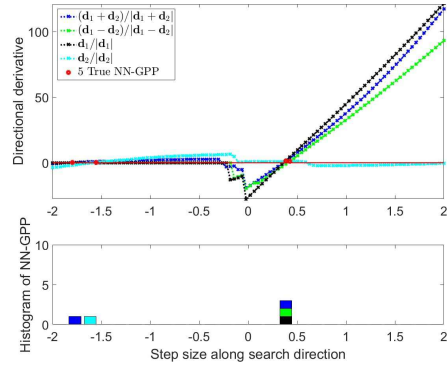
(c) Function value, $|\mathcal{B}| = 10$



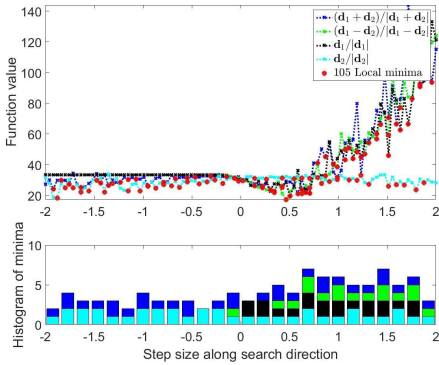
(d) Directional derivative, $|\mathcal{B}| = 10$



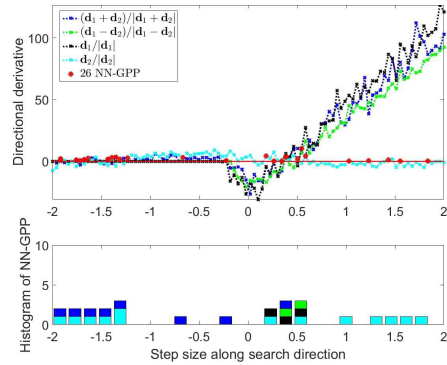
(e) True minima along search directions



(f) True NN-GPP along search directions

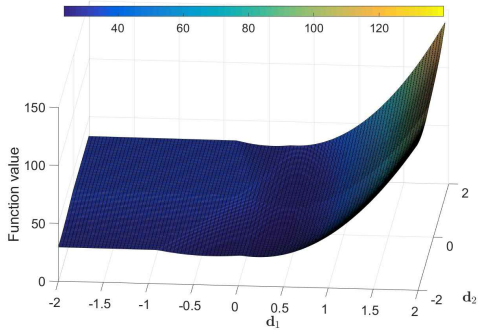


(g) Local minima along search directions

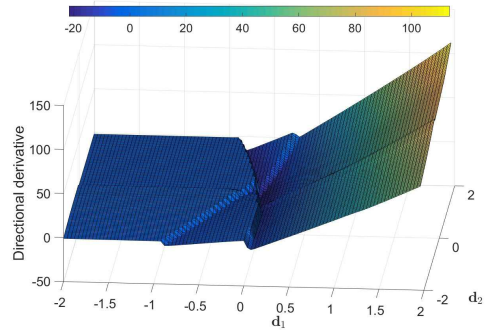


(h) NN-GPP along search directions

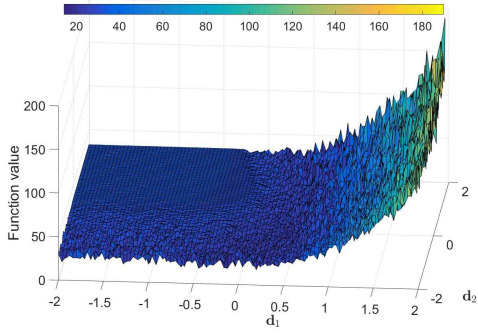
Figure 15: The ReLU activation function closeup: Notable features are the stark changes in the directional derivatives. These correspond to the "activation" and "deactivation" of various nodes in the network. A unique feature to the ReLU activation is the presence of flat planes with 0 directional derivative. These areas denote weight spaces where no information passes through the network, even in mini-batch settings.



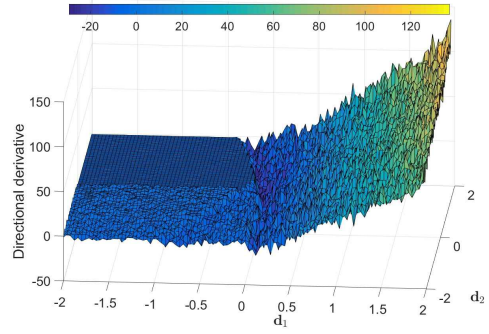
(a) Function value, $|\mathcal{M}| = 150$



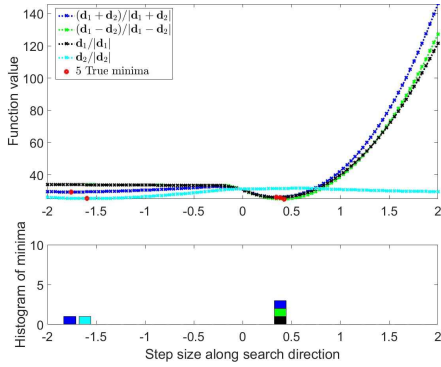
(b) Directional derivative, $|\mathcal{M}| = 150$



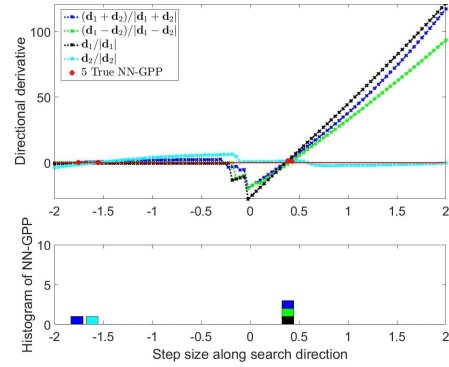
(c) Function value, $|\mathcal{B}| = 10$



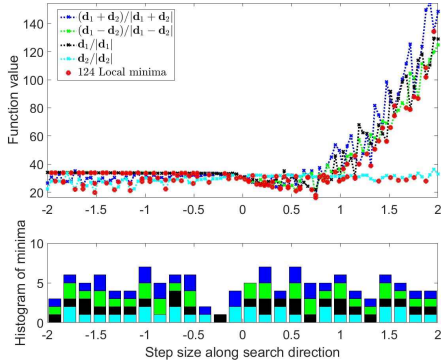
(d) Directional derivative, $|\mathcal{B}| = 10$



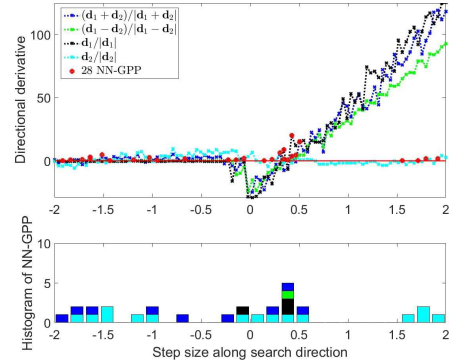
(e) True minima along search directions



(f) True NN-GPP along search directions

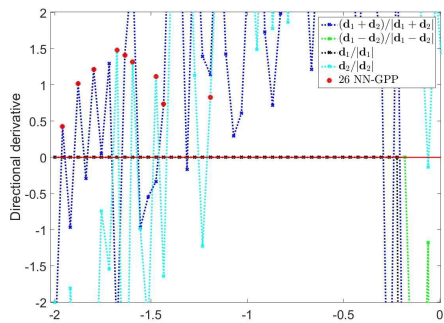


(g) Local minima along search directions

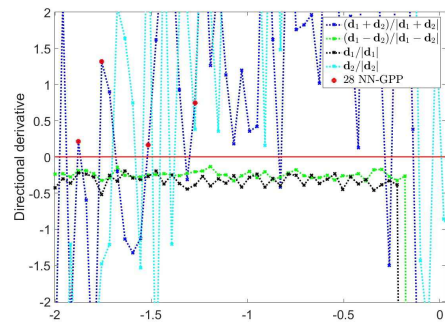


(h) NN-GPP along search directions

Figure 16: The leaky ReLU activation function closeup: Flat planes with constant directional derivative values are also present here. Although in this case they have a non-zero numerical value, they do not contribute significantly to localizing NN-GPPs or reducing the number of true optima for the ReLU class.

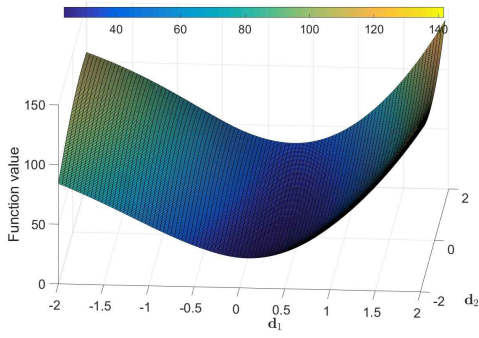


(a)

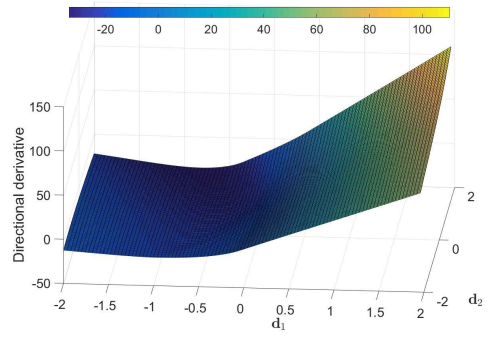


(b) Directional derivative, $|\mathcal{M}| = 150$

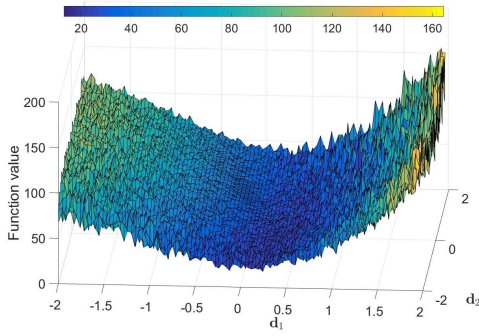
Figure 17: Detailed comparison of directional derivative plots between ReLU and leaky ReLU activations when hidden units become "inactive". As expected, ReLU units switch "off" entirely, containing no gradient information, while the leaky ReLU results in non-zero directional derivatives.



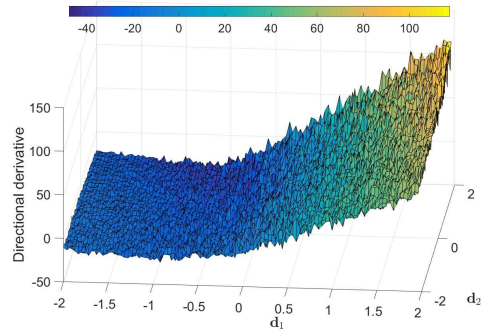
(a) Function value, $|\mathcal{M}| = 150$



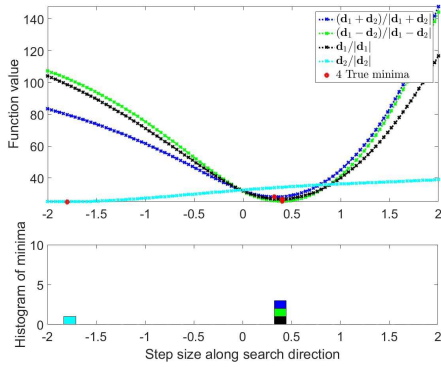
(b) Directional derivative, $|\mathcal{M}| = 150$



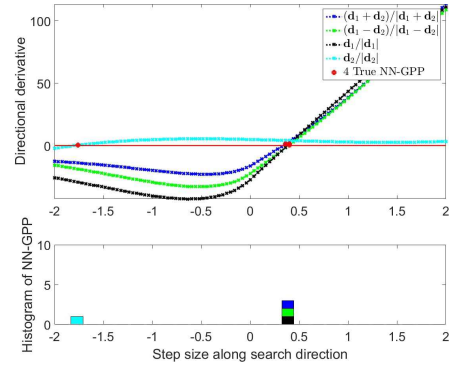
(c) Function value, $|\mathcal{B}| = 10$



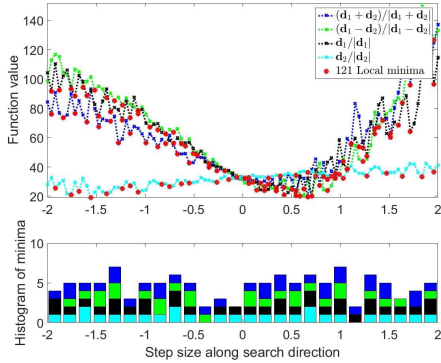
(d) Directional derivative, $|\mathcal{B}| = 10$



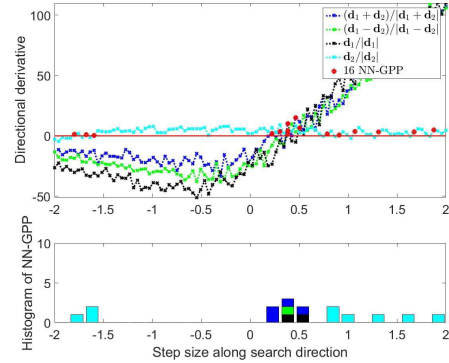
(e) True minima along search directions



(f) True NN-GPP along search directions



(g) Local minima along search directions



(h) NN-GPP along search directions

Figure 18: The ELU activation function closeup: The smooth exponential derivative in the negative domain of the activation function results in a greater magnitude in negative directional derivatives in the loss ((d) and (h)) compared to the remainder of its class. This in turn helps distance the directional derivatives from 0, localizing the sign changes for the higher curvature directions.

References

- A. Agarwal, P. L. Bartlett, P. Ravikumar, and M. J. Wainwright. Information-theoretic lower bounds on the oracle complexity of stochastic convex optimization. *IEEE Transactions on Information Theory*, 58(5):3235–3249, May 2012. ISSN 0018-9448. doi: 10.1109/TIT.2011.2182178.
- Jasbir Arora. *Introduction to Optimum Design, Third Edition*. Academic Press Inc, 2011. ISBN 0123813751.
- James Bergstra, Guillaume Desjardins, Pascal Lamblin, and Yoshua Bengio. Quadratic Polynomials Learn Better Image Features. *Technical Report 1337, IT Department and operations research, University of Montreal*, pages 1–11, 2009.
- Djork-Arne Clevert, Thomas Unterthiner, and Sepp Hochreiter. Fast and Accurate Deep Network Learning by Exponential Linear Units (ELUS). In *ICLR 2016*, pages 1–14, 2016. ISBN 9780996452700. doi: 10.23919/ICIF.2017.8009734.
- D. Csiba and P. Richtarik. Importance Sampling for Minibatches. *Journal of Machine Learning Research*, 19:1–21, 2018.
- John Duchi, Elad Hazan, and Yoram Singer. Adaptive Subgradient Methods for Online Learning and Stochastic Optimization. *Journal of Machine Learning Research*, 12 (Jul):2121–2159, 2011. ISSN 1533-7928. URL <http://jmlr.org/papers/v12/duchi11a.html>.
- Xavier Glorot and Antoine Bordes. Deep Sparse Rectifier Neural Networks. In *Proceedings of Machine Learning Research*, volume 15, pages 315–323, 2011. ISBN 1532-4435. doi: 10.1.1.208.6449.
- Ian J. Goodfellow, Oriol Vinyals, and Andrew M. Saxe. Qualitatively Characterizing Neural Network Optimization Problems. *ICLR*, pages 1–11, 2015. URL <http://arxiv.org/abs/1412.6544>.
- Daniel Jiwoong Im, Michael Tao, and Kristin Branson. An empirical analysis of the optimization of deep network loss surfaces. *arxiv*, pages 1–21, 2016. URL <http://arxiv.org/abs/1612.04010>.
- Dominic Kafka and Daniel Wilke. ‘Gradient-only line searches: An Alternative to Probabilistic Line Searches’. *Unpublished: To be submitted to ArXiv, Centre for Asset and Integrity Management, Department of Mechanical and Aeronautical Engineering, University of Pretoria*, pages 1–25, 2019.
- Bekir Karlik. Performance analysis of various activation functions in generalized MLP architectures of neural networks. *International Journal of Artificial Intelligence and Expert Systems*, 1(4):111–122, 2015.
- R.L. Kashyap, C.C. Blaydon, and K.S. Fu. 9 stochastic approximation. In J.M. Mendel and K.S. Fu, editors, *Adaptive, Learning and Pattern Recognition Systems*, volume 66 of *Mathematics in Science and Engineering*, pages 329 – 355. Elsevier, 1970. doi: [https://doi.org/10.1016/S0076-5392\(08\)60499-3](https://doi.org/10.1016/S0076-5392(08)60499-3). URL <http://www.sciencedirect.com/science/article/pii/S0076539208604993>.
- Diederik P. Kingma and Jimmy Ba. Adam: A Method for Stochastic Optimization. In *ICLR 2015*, pages 1–15, 2015. ISBN 9781450300728. doi: <http://doi.acm.org.ezproxy.lib.ucf.edu/10.1145/1830483.1830503>. URL <http://arxiv.org/abs/1412.6980>.

- Robert Kleinberg, Li Yuanzhi, and Yuan Yang. An Alternative View: When Does SGD Escape Local Minima? In *35th International Conference on Machine Learning (PMLR 80)*, pages 1–10, 2018.
- Antonino Laudani, Gabriele Maria Lozito, Francesco Riganti Fulginei, and Alessandro Salvini. On training efficiency and computational costs of a feed forward neural network: A review. *Computational Intelligence and Neuroscience*, 2015:1–13, 2015. ISSN 16875273. doi: 10.1155/2015/818243.
- Hao Li, Zheng Xu, Gavin Taylor, Christoph Studer, and Tom Goldstein. Visualizing the Loss Landscape of Neural Nets. *ICLR 2018 Conference*, 2018. URL <http://arxiv.org/abs/1712.09913>.
- Shiyu Liang, Ruoyu Sun, Jason D. Lee, and R. Srikant. Adding One Neuron Can Eliminate All Bad Local Minima. *NeurIPS2018*, 32(Nips), 2018. ISSN 1600-6143. doi: 10.1111/ajt.12036. URL <http://arxiv.org/abs/1805.08671>.
- Andrew L. Maas, Awni Y. Hannun, and Andrew Y Ng. Rectifier nonlinearities improve neural network acoustic models. In *ICML 2013*, volume 28, page 6, 2013. ISBN 0162-4962. doi: 10.1016/0010-0277(84)90022-2. URL http://www.stanford.edu/~awni/papers/relu_hybrid_icml2013_final.pdf.
- Maren Mahsereci and Philipp Hennig. Probabilistic Line Searches for Stochastic Optimization. pages 1–12, 2017. ISSN 10495258. doi: 10.1016/j.physa.2015.02.029. URL <http://arxiv.org/abs/1703.10034>.
- James Martens. Deep Learning via Hessian-free Optimization. In *ICML*, pages 1–6, 2010. URL http://www.cs.toronto.edu/~jasamir/cifar/HFO_James.pdf.
- D Masters and C Lusch. Revisiting Small Batch Training for Deep Neural Networks. 2018. URL <https://arxiv.org/abs/1804.07612>.
- Yurii Nesterov. A method of solving a convex programming problem with convergence rate $O(1/k^2)$. *Soviet Mathematics Doklady*, 27:372–376, 1983.
- Quynh Nguyen, Mahesh Chandra Mukkamala, and Matthias Hein. On the loss landscape of a class of deep neural networks with no bad local valleys. *arxiv*, pages 1–20, 2018. URL <http://arxiv.org/abs/1809.10749>.
- Herbert Robbins and Sutton Monro. A Stochastic Approximation Method. *The Annals of Mathematical Statistics*, 22(3):400–407, sep 1951. ISSN 0003-4851. doi: 10.1214/aoms/1177729586. URL <http://projecteuclid.org/euclid.aoms/1177729586>.
- Nicol N Schraudolph, Jin Yu, and Simon Günter. A Stochastic Quasi-Newton Method for Online Convex Optimization. *International Conference on Artificial Intelligence and Statistics*, pages 436–443, 2007. ISSN 15324435. doi: 10.1137/140954362. URL <http://eprints.pascal-network.org/archive/00003992/>.
- A Serwa. Studying the Effect of Activation Function on Classification Accuracy Using Deep Artificial Neural Networks. *Journal of Remote Sensing & GIS*, 06(03):6–11, 2017. doi: 10.4172/2469-4134.1000203.
- Naun Zuselevich Shor. Minimization Methods for Non-Differentiable Functions. chapter The Subgra, pages 22–47. Springer, Berlin Heidelberg, 1985. URL http://www.springerlink.com/index/10.1007/978-3-642-82118-9_3.
- Jan A Snyman and Daniel N Wilke. *Practical Mathematical Optimization*, volume 133 of *Springer Optimization and Its Applications*. Springer International Publishing, Cham, 2018. ISBN 978-3-319-77585-2. doi: 10.1007/978-3-319-77586-9. URL <http://link.springer.com/10.1007/978-3-319-77586-9>.

- Fei Tong and Xila Liu. Samples Selection for Artificial Neural Network Training in Preliminary Structural Design. *Tsinghua Science & Technology*, 10(2):233–239, apr 2005. ISSN 1007-0214. doi: 10.1016/S1007-0214(05)70060-2. URL <https://www.sciencedirect.com/science/article/pii/S1007021405700602>.
- Paul John Werbos. *The Roots of Backpropagation: From Ordered Derivatives to Neural Networks and Political Forecasting*. Wiley-Interscience, New York, NY, USA, 1994. ISBN 0-471-59897-6.
- P.J. Werbos. Applications of advances in nonlinear sensitivity analysis. In R.F. Drenick and F. Kozin, editors, *System Modeling and Optimization. Lecture Notes in Control and Information Sciences*, volume 38. Springer, Berlin, Heidelberg, 1982. ISBN 3-540-11691-5.
- Daniel N. Wilke, Schalk Kok, and Albert A. Groenwold. Relaxed error control in shape optimization that utilizes remeshing. *International Journal for Numerical Methods in Engineering*, 94(3):273–289, 2013a.
- Daniel Nicolas Wilke, Schalk Kok, Johannes Arnoldus Snyman, and Albert A. Groenwold. Gradient-only approaches to avoid spurious local minima in unconstrained optimization. *Optimization and Engineering*, 14(2):275–304, June 2013b. ISSN 1389-4420. doi: 10.1007/s11081-011-9178-7. URL <http://link.springer.com/10.1007/s11081-011-9178-7>.
- Chang Xu, Tao Qin, Gang Wang, and Tie-Yan Liu. Reinforcement Learning for Learning Rate Control. *arXiv*, 2017. URL <http://arxiv.org/abs/1705.11159>.